Soliton dynamics in frequency-modulated lattices

Author:
Sun, Yang

Publication Date:
2014

DOI:
https://doi.org/10.26190/unsworks/17082

SOLITON DYNAMICS IN FREQUENCY-MODULATED LATTICES

A thesis submitted for the degree of
Master of Philosophy

By
Yang Sun
M.E.

Applied and Industrial Mathematics Research Group,
School of Physical, Environmental and Mathematical Sciences,
The University of New South Wales,
Australian Defence Force Academy.

November 2014

I hereby declare that this submission is my own work and to the best of my knowledge it contains no material previously published or written by another person, nor material which to a substantial extent has been accepted for the award of any other degree or diploma at UNSW or any other educational institution, except where due acknowledgement is made in the thesis. Any contribution made to the research by colleagues, with whom I have worked at UNSW or elsewhere, during my candidature, is fully acknowledged.

I also declare that the intellectual content of this thesis is the product of my own work, except to the extent that assistance from others in the project's design and conception or in style, presentation and linguistic expression is acknowledged.

Yang Sun

Abstract

Currently, experimental and theoretical studies of solitons have been conducted in the context of several areas of science, from applied mathematics and physics to chemistry and biology. A significant amount of soliton research is concentrated on nonlinear optics (light waves) and Bose-Einstein condensates (matter waves) in optical lattices, which are often described by the Gross-Pitaevskii equation or the nonlinear Schrödinger equation with a periodic potential.

We studied soliton dynamics in both time-independent and time-dependent potentials. We used a variational approach to simplify the problem by reducing it to the study of the dynamics of a particle in an effective potential. We saw good agreement between the numerical and approximate variational solutions, indicating the variational method is a simple yet powerful method for the study of soliton dynamics in a frequency-modulated potential. We studied several scenarios, including soliton trapping by a periodic potential, 'jumping' between adjacent wells and parametric resonance. We also investigated the soliton dynamics by using Poincaré sections and histograms to examine the velocity distribution of the driven solitons for different initial conditions.

Acknowledgements

I would never have been able to finish my thesis without the guidance of my superviors, help from friends, and support from my family and girlfriend.

I would like to express my special appreciation to my superiors, Dr. Tristram Alexander, Dr. Isaac Towers and Dr. Zlatko Jovanoski, who are not only teachers but dear friends. The advice on both research as well as on my career are priceless. I appreciate they teach me how to use the resources to support my research (Web searching, books and software). They always inspire and encourage me to solve problems instead of giving me an answer, and allow me to grow as a research student. This is quite important for me so that I can feel my progress personally. As Chinese old saying: 'Give a man a fish and you feed him for a day. Teach a man to fish and you feed him for a lifetime.'

I also would like to thank all the colleagues in UNSW Canberra who have helped me. I appreciate all of my friends who supported me in writing to strive towards my goal.

A special thank goes to my family. Words cannot express how grateful I am to my family for all of the sacrifices. I would like express appreciation to my beloved dear girlfriend, Xinyan Huang, for being there to listen, to think and to make brilliant advices throughout entire process. Her prayer for me was what sustained me thus far.

Contents

Declaration ii

Abstract iii

Acknowledgements v

Chapter 1 Introduction 1

1.1 Our research 1
1.2 Background 1
1.2.1 What is a soliton? 1
1.2.2 Potentials 4
1.3 Solitons in potentials 5
1.4 Our research structure 7

Chapter 2 Methods and simple case results 9

2.1 Our research model 9
2.2 Methods 10
2.2.1 Exact solution discussion 10
2.2.2 Stationary solution 11
2.2.3 Numerical propagation 14
2.2.4 Variational approach 15
2.3 Results 17
2.3.1 Time-independent parabolic potential. 17
2.3.2 Time-independent periodic potential. 18
2.4 Conclusion 20

Chapter 3 Time-dependent frequency-modulated potential. 23

3.1 Time-dependent potential. 23
3.2 Non-resonance dynamics 24
3.2.1 Oscillation in the minima of the potential. 24
3.2.2 Motion between potential wells. 24
3.2.3 Initial condition 26
3.3 Parametric resonance 28

3.3.1 Poincaré section and histogram 31
3.4 Asymmetric potential 32
3.5 Damping 36
3.6 Conclusion 39

Chapter 4 Conclusion and future work 41
4.1 Concluding remarks 41
4.2 Future work 42
4.2.1 Characterisation of velocity probability distribution 42
4.2.2 Exploration of dynamics for different values of the parameters 42
4.2.3 Emergence of directed transport for particle 42
4.2.4 Stochastic variations in the period of the lattice 43

Appendix A Matlab code 49
A.1 Numerical method (PDE) 49
A.2 Variational approach (ODE) 49

Appendix B Numerics 51

List of Figures

1.1 Schematic plots of the soliton solutions of three famous nonlinear wave equations [1]. 4

1.2 (a) A one-dimensional optical lattice created from counterpropagating laser beams; (b) with beams enclosing an angle θ. The parameters V_0 and d are the lattice depth and lattice spacing respectively [2]. . . 6

2.1 No potential applied, $W(x,t) = 0$. 11

2.2 Time-independent parabolic potential, $W(x,t) = \frac{1}{2}\omega_0^2 x^2$, $\omega_0 = \sqrt{0.2}$. . 12

2.3 Time-independent periodic potential, $W(x,t) = -\cos(k_0 x)$, $k_0 = 0.5$, $k_{mod} = 0$. 13

2.4 Exact lowest order stationary soliton solution of the nonlinear Schrödinger equation. $A = 1/w = \sqrt{2\alpha} = 4$ 14

2.5 Max $|\psi|$ propagation with time in the parabolic potential. The varying of Max $|\psi|$ is small. The soliton width ($w = 0.25$). 18

2.6 Dynamics in a parabolic potential with $\omega_0 = \sqrt{0.2}$, $x_0 = 2$ and $\dot{x}_0(0) = 0$. Parameters: $L = 5$, $N = 2^8$, $\Delta x = 2L/N$, $\Delta t = 0.0015$,the actual value of the maximum error: 6.7699×10^{-4}. The soliton in a parabolic potential in (a), (c) and the comparison results from ODE (the central white line in figure (b) and (c)) and PDE methods in (b),(d). We can see the differences in position between PDE and ODE results in figure (d). 19

2.7 Max $|\psi|$ propagation with time in a periodic potential. The soliton width ($w = 0.25$). The varying of Max $|\psi|$ is small. $W(x,t) = -\cos[k_0 + k_{mod}\sin(\eta t)]x$, $k_0 = 0.5$, $k_{mod} = 0$, and $x_0 = 2$. 20

2.8 Dynamics in a time-independent periodic potential with $k_0 = 0.5$, $x_0 = 2$ and $\dot{x}_0(0) = 0$. Parameters: $L = 10$, $N = 2^8$, $\Delta x = 2L/N$, $\Delta t = 0.0015$, the actual value of the maximum error: 6.8701×10^{-4}. Comparison between the variational solution (b) and that of the numerical solution (c) is shown in (d). 21

3.1 (a) shows the comparison of results from numerical method and variational approach (the central white line in figure (a)), the potential $W(x,t) = -\cos[k_0 + k_{mod}\sin(\eta t)]x$. The initial condition are: $x_0 = 3.5$, $k_0 = 0.5$, $k_{mod} = 0.05$, $\eta = 0.1$. The particle-like soliton is trapped in the blue area which presents the lower density of the potential. (red and blue correspond to the maxima and minima of the potential respectively) In figure 3.1 (b), we can see the differences in position between PDE and ODE results. 24
3.2 Comparison the results of numerical method and variational approach (the central white line) in the potential $W(x,t) = -\cos[k_0 + k_{mod}\sin(\eta t)]x$. The initial condition are: $x_0 = 3.5$, $k_0 = 0.5$, $k_{mod} = 0.05$, $\eta = 0.1$. . . 25
3.3 Jumping case with potential and the initial conditions are: $x_0 = 6$, $k_0 = 0.5$, $k_{mod} = 0.05$, $\eta = 0.1$. In figure (a), the central white line presents the result from variational approach. In figure (b), we can see the differences in position between PDE and ODE results. . . . 25
3.4 Comparison the results of numerically solving PDE and variational approach (the central white line) in the potential $W(x,t) = -\cos[k_0 + k_{mod}\sin(\eta t)]x$. The initial condition are: $x_0 = 6$, $k_0 = 0.5$, $k_{mod} = 0.05$, $\eta = 0.1$. . . 26
3.5 A couple of value figures which shows the final positions in (a) and final velocities in (b) for different initial conditions at a time equal to 10 times the force period. Parameters: $-6 \leqslant x_0 \leqslant 6, -3 \leqslant v_0 \leqslant 3, k_0 = 0.5, k_{mod} = 0.05, \eta = 0.1, 0 \leqslant t \leqslant 20\pi/\eta$. 26
3.6 Poincare map created by sampling 1000 ODE solutions from $t = 0$ to $t = 2000$ every $t = 2\pi/\eta$. Quasi-periodic trapped solutions are evident as circles, chaotic motion appears as disconnected dots. Parameters of time-dependent potential: $-40 \leqslant x_0 \leqslant 40$, $-4 \leqslant v_0 \leqslant 4$, $k_0 = 0.5$, $k_{mod} = 0.05$ and $\eta = 0.1$. 27
3.7 A histogram of velocities. (a) shows the velocity frequencies in 100 intervals within velocity range. The vertical axis of (b) is logarithmic (base 10) scale of the vertical axis in figure (a) Parameters: $x_0 = 6, v_0 = 3, k_0 = 0.5, k_{mod} = 0.05, \eta = 0.1, 0 \leqslant t \leqslant 10000$. 28
3.8 A histogram of velocities. The velocity frequencies in 100 intervals within velocity range. Parameters: $k_0 = 0.5, k_{mod} = 0.05, \eta = 0.1, x_0 = 2, v_0 = 4, 0 \leqslant t \leqslant 50000$. 29
3.9 A histogram of velocities. The velocity frequencies in 100 intervals within velocity range. Parameters: $k_0 = 0.5, k_{mod} = 0.05, \eta = 0.1, x_0 = 2, v_0 = 10, 0 \leqslant t \leqslant 80000$. 29

3.10 A histogram of velocities. The velocity frequencies in 100 intervals within velocity range. Parameters: $k_0 = 0.5, k_{mod} = 0.05, \eta = 0.1, x_0 = 4, v_0 = 2, 0 \leqslant t \leqslant 50000$. 30
3.11 A histogram of velocities. Parameters: $k_0 = 0.5, k_{mod} = 0.05, \eta = 0.1, -40 \leqslant x_0 \leqslant 40, -4 \leqslant v_0 \leqslant 4$. 30
3.12 A histogram of velocities. Parameters: $k_0 = 0.5, k_{mod} = 0.05, \eta = 0.1, -10 \leqslant x_0 \leqslant 10, -2 \leqslant v_0 \leqslant 2, 0 \leqslant t \leqslant 10000$. 31
3.13 The upper figure shows that the comparison of numerical method and variational approach (the central white line). The lower figure illustrates the trajectory of the particle. The initial condition is $x_0 = 0.5$, $k_0 = 0.5$, $k_{mod} = 0.05$, $\eta = 1$ and $\Omega = 0.498398$. 32
3.14 Poincare map created from $t = 0$ to $t = 600$ every $t = 2\pi/\eta$. Quasi-periodic trapped solutions are evident as circles, chaotic motion appears as disconnected dots. Parameters of time-dependent potential: $-20 \leqslant x_0 \leqslant 20$, $-2 \leqslant v_0 \leqslant 2$, $k_0 = 0.5$, $k_{mod} = 0.05$ and $\eta = 1$. . . . 33
3.15 A histogram of a set of initial conditions for velocities. Parameters: $k_0 = 0.5, k_{mod} = 0.05, \eta = 1, -20 \leqslant x_0 \leqslant 20, -2 \leqslant v_0 \leqslant 2, 0 \leqslant t \leqslant 600$. 33
3.16 The regular symmetry potential (a) and the asymmetric potential (b) and (c). 34
3.17 Poincare section of a soliton in an asymmetric potential. The potential is $W(x,t) = -\cos(k(t)x)$, $k(t) = k_0 + k_{mod}(\sin(\eta t) - 0.3\sin(2\eta t))$. The initial condition ranges are $-20 \leqslant x_0 \leqslant 20$, $-2 \leqslant v_0 \leqslant 2$, sampling by every $t = 2\pi/\eta$ 34
3.18 The trajectories of a soliton in an asymmetric potential. The potential is $W(x,t) = -\cos(k(t)x)$, $k(t) = k_0 + k_{mod}(\sin(\eta t) - 0.3\sin(2\eta t))$. The initial condition ranges are $-20 \leqslant x_0 \leqslant 20$, $-2 \leqslant v_0 \leqslant 2$ sampling by every $t = 2\pi/100\eta$, $\eta = 0.1$. 35
3.19 Soliton in the regular symmetry potential 3.16(a). The initial condition: $x_0 = 2$, $v_0 = 1$, (a) and (b) are trajectories of x and v respectively, (c) displays the Poincaré section sampling by every $t = 2\pi/\eta$, $\eta = 0.1$ during $t = 12000$. (d) shows the histogram of velocities. . . 36
3.20 Soliton in the asymmetric potential 3.16(b). The initial condition: $x_0 = 2$, $v_0 = 1$, (a) and (b) are trajectories of x and v respectively, (c) displays the Poincaré section sampling by every $t = 2\pi/\eta$, $\eta = 0.1$ during $t = 12000$. (d) shows the histogram of velocities. 36

3.21 Soliton in the asymmetric potential 3.16(c). The initial condition: $x_0 = 2$, $v_0 = 1$, (a) and (b) are trajectories of x and v respectively, (c) displays the Poincaré section sampling by every $t = 2\pi/\eta$, $\eta = 0.1$ during $t = 12000$. (d) shows the histogram of velocities. 37
3.22 The damping case which initial condition: $x_0 = 2$, $v_0 = 1$ and $t = 500$, (a) and (b) are trajectories of x and v respectively, (c) displays the Poincaré section sampling by every $t = 2\pi/\eta$, $\eta = 0.1$. (d) shows the histogram of velocities. 37
3.23 The damping case which initial condition: $x_0 = 2$, $v_0 = 1$ and $t = 500$ (a) and (b) are trajectories of x and v respectively, (c) displays the trajectories sampling by every $t = 2\pi/100\eta$, $\eta = 0.1$. (d) shows the histogram of velocities. 38
3.24 The damping case which initial condition: $x_0 = 6$, $v_0 = 1$ and $t = 500$ (a) and (b) are trajectories of x and v respectively, (c) displays the Poincaré section sampling by every $t = 2\pi/\eta$, $\eta = 0.1$. (d) shows the histogram of velocities. 38
3.25 The damping case which initial condition: $x_0 = 1$, $v_0 = 4$ and $t = 500$ (a) and (b) are trajectories of x and v respectively, (c) displays the Poincaré section sampling by every $t = 2\pi/\eta$, $\eta = 0.1$. (d) shows the histogram of velocities. 39
B.1 No potential. The soliton width range $(0.125 - 2.5)$ 52
B.2 No potential. The soliton width range $(0.125 - 0.5)$ 53
B.3 Time-independent parabolic potential. The soliton width range $(0.125-2.5)$. 54
B.4 Time-independent parabolic potential. The soliton width range $(0.125-0.5)$. 55
B.5 Time-independent parabolic potential. The soliton width range $(1-2.5)$. 55
B.6 Time-independent periodic potential. The soliton width range $(0.125-2.5)$. 56
B.7 Time-independent periodic potential. The soliton width range $(0.125-0.5)$. 57
B.8 Time-independent periodic potential. The soliton width range $(1-2.5)$. 57
B.9 Time-independent periodic potential. The soliton width $(w = 0.25)$. $W(x,t) = -\cos[k_0 + k_{mod}\sin(\eta t)]x$, $k_0 = 0.5$, $k_{mod} = 0$, and $x_0 = 2$. 57
B.10 Time-independent periodic potential. The soliton width range $(w = 0.25)$. $W(x,t) = \frac{1}{2}\omega_0^2 x^2$, $\omega_0 = \sqrt{0.2}$ and $x_0 = 2$ 57

Chapter 1

Introduction

A characteristic of solitons is that they can travel long distances in space and (or) time with very little loss of energy and structure. Precisely because of this quality, soliton theory can be widely applied in numerous branches of science and technology, such as optical communication, electronic devices, biology etc. However, though systems with external potentials make difficult the development of solitons applications, potentials open up more possibilities for the control of solitons . Thus, the study of solitons in potentials is valuable.

This introductory chapter is intended to provide a general overview of our research. The research presented in this thesis is the study of soliton dynamics in a time-dependent potential.

1.1 Our research

We use a spatially periodic potential which is periodically modulated in time. This modulation involves changing the spatial period (or frequency). We use a variational approach to obtain a simpler ordinary diferential equation model of the soliton dynamics and verify that the predicted dynamics agrees with the full model. We use both models to study the system and reveal the possibility of soliton trapping and chaotic soliton tunnelling.

In the next section, we present background information concerning the history and characteristics of solitons and potentials.

1.2 Background

1.2.1 What is a soliton?

The term 'soliton' was introduced by Zabusky and Kruskal to name waves which maintain their shape and velocities after collision in numerical calculations they performed [3]. The name soliton is meant to suggest the idea of a particle like the terms 'proton', 'electron', etc. However, they were not the first to discover the soliton. An observation was made in a canal near Edinburgh by John Scott Russell in the 1830s which he called a 'Wave of Translation'. He described the properties of the wave in his report [4]:

> I believe I shall best introduce the phaenomenon by describing the circumstances of my own first acquaintance with it. I was observing the motion of a boat which was rapidly drawn along a narrow channel by a pair of horses, when the boat suddenly stopped-not so the mass of water in the channel which it had put in motion; it accumulated round the prow of the vessel in a state of violent agitation, then suddenly leaving it behind, rolled forward with great velocity, assuming the form of a large solitary elevation, a rounded, smooth and well-defined heap of water, which continued its course along the channel apparently without change of form or diminution of speed. I followed it on horseback, and overtook it still rolling on at a rate of some eight or nine miles an hour, preserving its original figure some thirty feet long and a foot to a foot and a half in height. Its height gradually diminished, and after a chase of one or two miles I lost it in the windings of the channel.

A soliton is a nonlinear wave which travels with permanent form and speed during propagation, even on interaction with other solitons [5]. In this work we focus on a particular type of soliton known as the bright soliton, which appears as a nonlinearly localized wave with a local maximum and asymptotically zero tails.

Mathematical solitons

Mathematically speaking, a soliton is a localised solution of a nonlinear, integrable, partial differential equation (PDE) with nonlinear stability properties. Solitons pass through each other without suffering any permanent change in form. An integrable PDE is solvable by the inverse scattering transform method [6]. The inverse scattering method is essentially an extension of Fourier transformation applied to nonlinear problems. Drazin and Johnson ascribe three properties to solitons [7]:

- They are of permanent form;
- They are localised within a region;
- They can interact with other solitons, and emerge from the collision unchanged, except for a phase shift.

Recently, more than one hundred different nonlinear partial differential equations exhibit soliton-like solutions [8]. Three famous integrable nonlinear equations that allow soliton solutions are shown in Fig 1.1:

- Two Dutch physicists, Korteweg and de Vries presented their now famous equation (KdV) in 1895 [9], which describes the propagation of waves on the surface of a shallow channel.

$$\frac{\partial\psi}{\partial t} - 6\psi\frac{\partial\psi}{\partial x} + \frac{\partial^3\psi}{\partial x^3} = 0.$$

- The Sine-Gordon equation (SG) originates from differential geometry, in which it describes a certain kind of surface [5].

$$\frac{\partial^2\psi}{\partial t^2} - \frac{\partial^2\psi}{\partial x^2} + \sin\psi = 0.$$

- The Nonlinear Schrödinger equation (NLSE)

$$i\frac{\partial\psi}{\partial t} + \frac{1}{2}\frac{\partial^2\psi}{\partial x^2}\psi + |\psi|^2\psi = 0,$$

  For which the solution is the envelope (i.e. like the KdV solution), in Fig. 1.1 (c). The NLSE description of the combined effects of dispersion and the non-linearity self-phase modulation, gave rise to envelope solitons. The first papers devoted to the NLSE in nonlinear optics appeared as early as 1964 [10]. Throughout our research we use the NLSE and variants of it to study soliton dynamics. The research model discussion is provided in the next chapter.

Physical solitons

In the physical world, there are always losses. Solitary waves are localised within a region. However, two initially separated solitary waves approach each other deforming their shapes as they collide and have different properties after collision, such as shapes, sizes or even producing radiation. If a train of physical solitons was transmitted in an optical fibre for a great distance, they must be amplified to compensate for the energy dissipation.

Some physical situations can be described by mathematical equations. Integrable models are still used to explain and solve the problem of physical soliton dynamics. Pulse solitons such as solitons in shallow water are described by the KdV [9] and the NLSE and the Gross-Pitaevskii Equation (GPE) have been applied in a wide variety of physical contexts, for instance, deep water [11], optics [12], and matter waves [13]. The Sine-Gordon equation has been used to model the propagation of crystal dislocations [14].

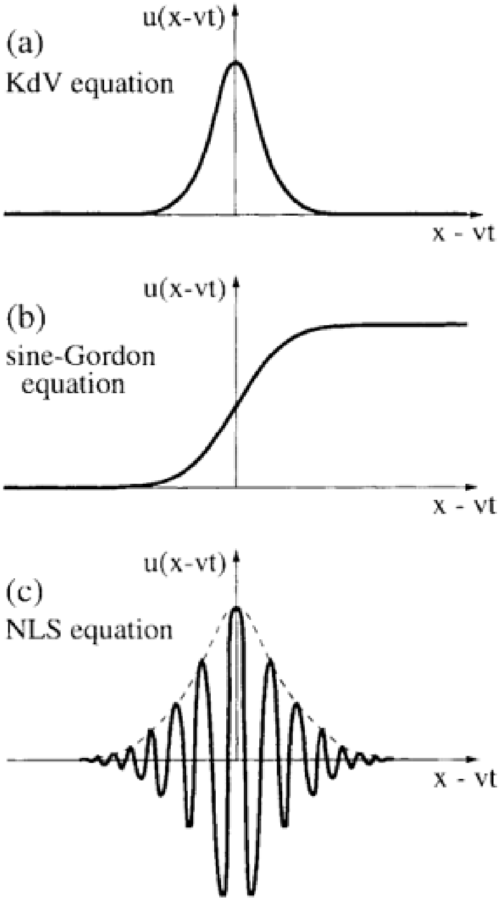

Figure 1.1: Schematic plots of the soliton solutions of three famous nonlinear wave equations [1].

1.2.2 Potentials

In physics, potential energy is the energy of position or the energy of formation [15]. An object with potential energy has the capability to do work even when it is static. Therefore, solitons in a potential possess potential energy. Two physical types of potentials are nonlinear optical media and the trapping mechanism of BEC experiments. BECs are a state of matter of a dilute gas of bosons cooled to temperatures very near absolute zero. Einstein predicted that cooling bosonic atoms to a very low temperature would cause them to fall (or "condense") into the lowest accessible quantum state, resulting in a new form of matter. This phenomenon was demonstrated for the first time in 1995 in ultracold vapors of alkali metals, [16–18].

The NLSE with a potential take the general form [19]:

$$i\frac{\partial\psi}{\partial t}+\frac{1}{2}\frac{\partial^2\psi}{\partial x^2}\psi-W(x,t)\psi+|\psi|^2\psi=0 \tag{1.1}$$

The term W is the external potential. The external potential may have many forms, such as the optical lattice potential (a periodic potential), and harmonic oscillator potential. Assuming $W = x^2$, the equation (1.1) describes a soliton in a harmonic potential. In this case, the soliton is trapped by the potential. Further discussion of dynamics in time-independent potentials is presented in section 2.3.

1.3 Solitons in potentials

The bright soliton is well-known in nonlinear fiber optics [20], where it can appear in a material with a self-focusing nonlinearity, and in Bose-Einstein condensates (BECs) [21], where it can appear in the presence of attractive atom-atom interactions. Our interest centres on the particle-like nature of the soliton. We explore the possibility of manipulating the soliton position through an external potential which varies during propagation. Our study is of most physical relevance to the BEC context, where the properties of an external potential may be flexibly controlled through the interference of lasers [2].

In BECs, the spatially periodic external potentials induce a corresponding modulation pattern of the local nonlinearity through the Feshbach-resonance mechanism, which produce the nonlinearity in the BECs [22]. In optics, periodic optical lattices generated by the interference of intersecting laser beams, which forms an optical standing wave with period trapping the solitons [23]. Such a time-varying potential is inspired by the optical lattices used in BEC experiments [2] in Fig.1.2. Such lattices (in one dimension) are typically constructed through the overlap of two coherent light fields, with the angle between the phase fronts of these fields determining the period of the lattice [2]. Thus if this angle is varied, the period of the lattice will vary. This variation could be easily achieved by changing the angle of a reflecting mirror (typically used so that only one laser source is needed). Introducing a time-periodic drive to this angle would then translate into a time-dependent (periodically modulated) lattice period. In many ways this is much simpler than previously considered time-periodic lattices (such as the modulations considered in [24]). Our work is thus on the one hand a first exploration of what this simple experimental arrangement brings, and on the other an investigation into a fundamentally new potential in which the variation is highly spatially dependent. Near the crossing point of the light fields only the period changes, however moving away from this crossing the minima of the potential also move spatially with time, with this shift becoming more pronounced the further away from the crossing we move. There is thus a natural 'centre' to the potential, breaking the symmetry of the time-independent problem.

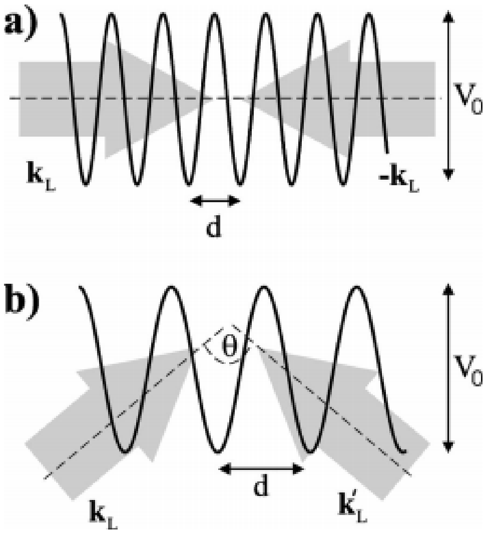

Figure 1.2: (a) A one-dimensional optical lattice created from counterpropagating laser beams; (b) with beams enclosing an angle θ. The parameters V_0 and d are the lattice depth and lattice spacing respectively [2].

The dynamics of BECs in time-dependent potentials has received an increasing amount of interest in recent years due to the possibility of precise experimental control. BECs have been successfully applied in a optical periodic potential based on the solution of the mean-field NLSE [25]. Researchers also investigated the dynamics of a bright soliton of BECs with time-varying atomic scattering length in a time-varying external parabolic potential [26]. The results show that it is controllable of the soliton's parameters (amplitude, width, and period). Double parametric resonance for matter-wave solitons in a time-periodic modulation trap, was also discussed in 2005 [27]. A variational approach was applied to study the center-of-mass coordinate of the soliton. In previous work, the longitudinally modulated potentials was studied in terms of phase space analysis for an effective particle approach and direct numerical simulations [24]. Further, a time-dependent confining harmonic oscillator potential was investigated by using two complementary methods: the adiabatic perturbation theory and direct numerical experiments [28]. Periodically changing the depth of the potential about zero was shown to lead to a ratchet-type effect for bright solitons [19] and even soliton control in two-dimensions [29]. More recently, more complicated types of periodic potential modulation have been proposed, including amplitude and wavenumber modulations [24]. However, very little is known about the soliton dynamics in frequency-modulated time-varying potential. Thus, we consider a new type of time-dependent modulation in this work: a periodic potential with a periodically varying frequency.

1.4 Our research structure

The aim of our research is to study the dynamics of a soliton in a time-dependent potential. Generally, we organized our research in two parts: (i) solitons in a time-independent potential; (ii) solitons in a time-dependent potential.

Chapter 2 introduces our research model and methods including the numerical method and the variational approach . We start to investigate soliton dynamics numerically in section 2.2.3. Furthermore, an effective particle approach [30] is applied in section 2.2.4, so that we obtain an ordinary differential equation (ODE) system describing soliton 'centre of mass' dynamics. This provides a significant reduction in the numerical load of approaching the PDE problem. In section 2.3, we verify our methods in a simpler time-independent potential case.

Chapter 3 discusses a more complex scenario: soliton in a time-dependent potential. We analyse the system by parameter modulated. In section 3.2, we present the non-resonance dynamics results depending on initial condition regulation. Then, we modulated the frequency to obtain a parametric resonance in section 3.3. In the following two sections 3.4 and 3.5, we study the soliton dynamics in an asymmetric potential and a damping situation.

Chapter 4 summarizes the remarkable results drawn from this research and recommends the future work.

Chapter 2

Methods and simple case results

This chapter is to introduce our research model and methods. We examine the suitable conditions for the numerical method and the variational approach, and then present and compare these two methods in details in section 2.2. After that, we apply the two methods to simple time-independent potentials in section 2.3.

2.1 Our research model

The NLSE is very important in mathematics, as well as in physics and engineering. The equation can be applied to hydrodynamics, nonlinear optics, nonlinear acoustics, BECs, heat pulses in solids and various other nonlinear instability phenomena. The $(1+1)$ dimensional NLSE that describes the propagation of a wave through an inhomogeneous nonlinear medium is given by [19]

$$i\frac{\partial\psi}{\partial t}+\frac{1}{2}\frac{\partial^2\psi}{\partial x^2}-W(x,t)\psi+|\psi|^2\psi=0. \tag{2.1}$$

Here $W(x,t)$ is the potential and ψ is the complex wave function. The second-order derivative represents diffraction, while $|\psi|^2\psi$ captures the nonlinear self-focusing of the wave. Our goal is to study the soliton dynamics in the presence of a time dependent periodic potential $W(x,t)$, specifically a frequency modulated potential of the form

$$W(x,t)=-\cos\left[k(t)x\right]\,,\quad k(t)=k_0+k_{mod}\sin(\eta t)\,, \tag{2.2}$$

where k_0 gives the base 'frequency' of the potential (the spatial period of the periodic potential is given by $T=2\pi/k_0$), k_{mod} is the maximum change in this base frequency and η gives the frequency at which the base frequency is modulated. This potential is inspired by the optical lattices used in BEC experiments. Such lattices (in one dimension) are typically constructed through the overlap of two coherent light fields, with the angle between the phase fronts of these fields determining the period of the lattice [2]. Thus, if this angle is varied the period of the lattice will vary. Such a setup could be easily achieved by changing the angle of a reflecting mirror as stated in chapter 1.

2.2 Methods

This work aims to study soliton dynamics in a potential. In this chapter, we introduce two methods, 'numerical propagation' and 'variational approach', for studying the soliton dynamics. We begin by developing our methods in the simpler case of a time-independent potential in section 2.3. We will consider the time-dependent case separately in the chapter 3.

2.2.1 Exact solution discussion

In this section, we check the approximation to determine if the exact solution of the NLSE (2.4) can be used as the stationary solution of the NLSE with a variety of potentials. We studied our model with no potential, then with two simple time-independent potentials. The main idea is to study if the $M = \mathrm{Max}|\psi|$ is varying with time propagation, which is a measurement of the approximation. If it is not a constant, the assumption does not apply to the model.

For instance, in figure 2.1(a), 2.2(a), 2.3(a) and 2.1(c), 2.2(c), 2.3(c) we see the variations in amplitude with time indicate some deviation of the initial conditions from the Eq.(2.3) stationary solution. We made a further investigation by calculating the difference δ, defined as:

$$\delta = \mathrm{Max}(M) - \mathrm{Min}(M). \tag{2.3}$$

There must be a maximum and a minimum value when the M is changing. So this δ is the difference between the maximum and minimum value. As the "δ" is close to zero, or even equals to zero, which is suggesting our assumption can be served well to our model. In figure 2.1(b), it is clear that most of "δ" are close to zero, except the width range ($w = 0.125 \sim 0.5$). After decreasing the space grid size $\Delta x = 2L/N$, we find that δ becomes smaller, as figure 2.1(d). Therefore, we can decrease this numerical error by improving the resolution of our calculations.

There are two parameter regions with large δ values when solitons propagated in the two simple time-independent potentials, as shown in figure 2.2(b) and 2.3(b). One is when the soliton has small width. The δ is increasing as the width is decreasing. But this numerical error can be diminished by improving calculation accuracy, as demonstrated in figure 2.2(d) and 2.3(d). The δ increases again when the soliton becomes wider than a certain value (Fig.2.2(e) and Fig.2.3(e)). This error cannot be avoided even with improved resolution of calculations, see figure 2.2(f) and 2.3(f). Therefore, we use the NLSE soliton with large width in time-dependent potentials we cannot treat it as a stationary solution. This suggests that the soliton width should be smaller than the external potential scale. By the data shows in Appendix

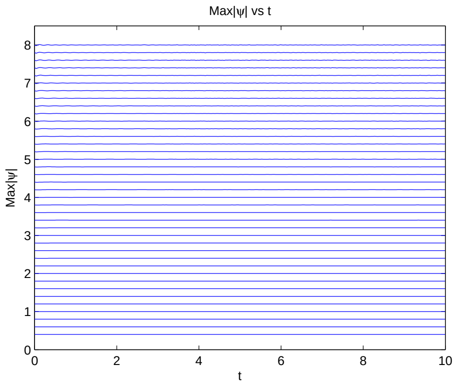

(a) Max $|\psi|$ propagation with time. The soliton width range $(0.125 - 2.5)$. Each line represents different widths. $\Delta x = 2L/N$, $L = 10$, $N = 2^{10}$.

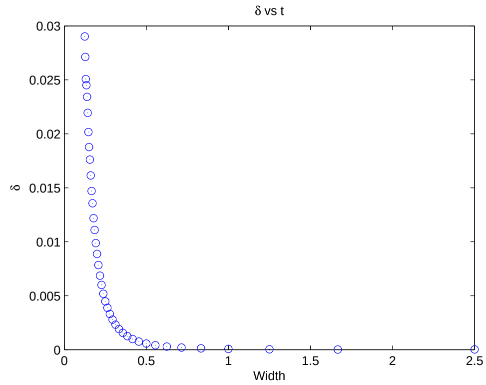

(b) Max $|\psi|$ varying range (δ) vs the width of soliton.

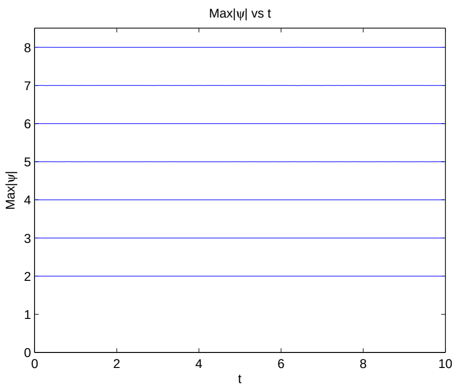

(c) Improved accuarcy of Max $|\psi|$ propagation with time. The soliton width range $(0.125 - 0.5)$. Each line represents different widths. $\Delta x = 2L/N$, $L = 10$, $N = 2^{12}$.

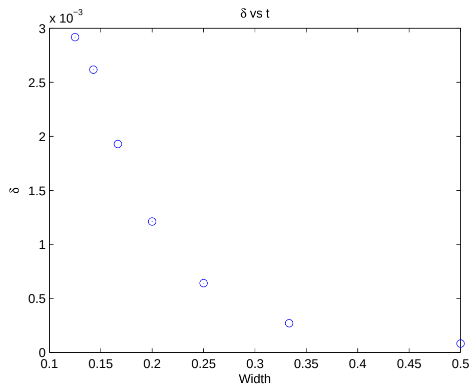

(d) Improved accuarcy of Max $|\psi|$ varying range (δ) vs the width of soliton.

Figure 2.1: No potential applied, $W(x,t) = 0$.

B, it suggests our assumptions are valid within soliton width less than 0.5 in time-independent potentials.

2.2.2 Stationary solution

The system (2.1) is nonintegrable and thus does not possess soliton solutions in the mathematical sense, however, we expect to find a family of localized soliton-like stationary solutions located at each minimum of the periodic potential. Such solutions must typically be found either numerically or through variational methods. However, if we consider only highly localized solutions then we may approximate

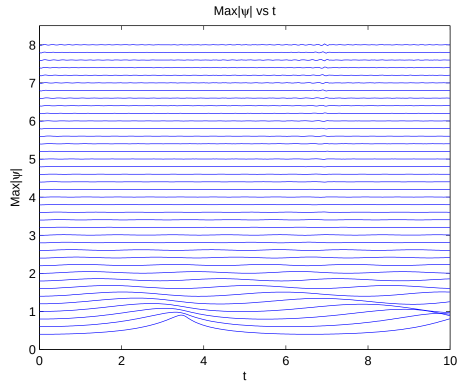

(a) Max $|\psi|$ propagation with time. The soliton width range $(0.125 - 2.5)$. Each line represents different widths. $\Delta x = 2L/N$, $L = 10$, $N = 2^{10}$.

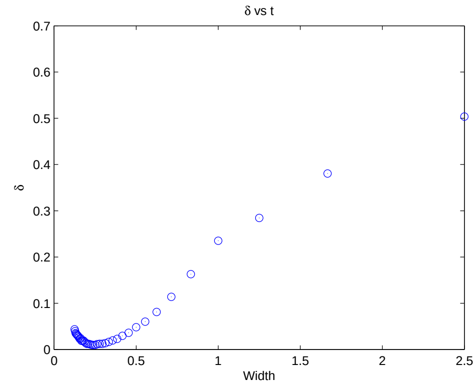

(b) Max $|\psi|$ varying range (δ) vs the width of soliton

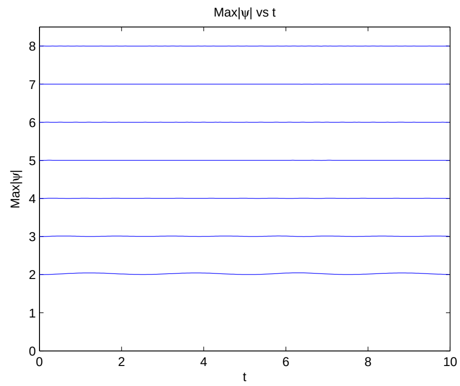

(c) Improved accuarcy of Max $|\psi|$ propagation with time. The soliton width range $(0.125 - 0.5)$. Each line represents different widths. $\Delta x = 2L/N$, $L = 10$, $N = 2^{12}$.

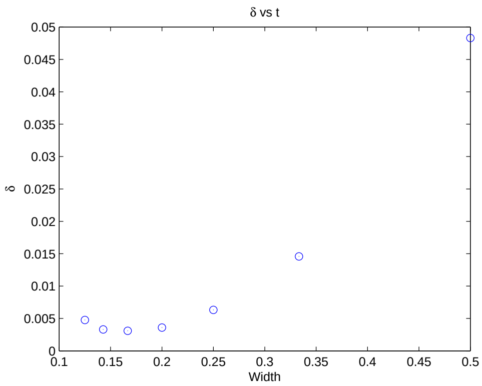

(d) Improved accuarcy of Max $|\psi|$ varying range (δ) vs the width of soliton

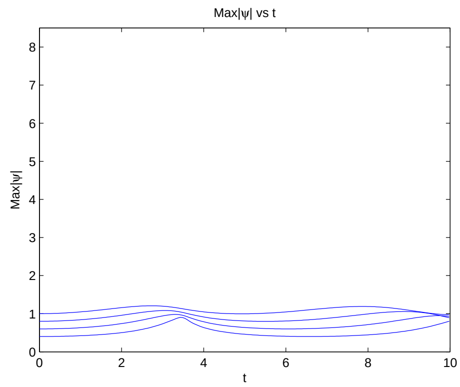

(e) Improved accuarcy of Max $|\psi|$ propagation with time. The soliton width range $(1 - 2.5)$. Each line represents different widths. $\Delta x = 2L/N$, $L = 10$, $N = 2^{12}$.

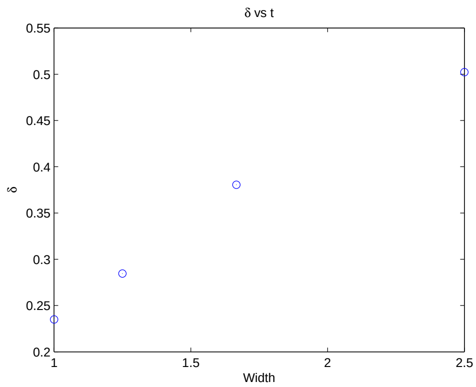

(f) Improved accuarcy of Max $|\psi|$ varying range (δ) vs the width of soliton

Figure 2.2: Time-independent parabolic potential, $W(x,t) = \dfrac{1}{2}\omega_0^2 x^2$, $\omega_0 = \sqrt{0.2}$.

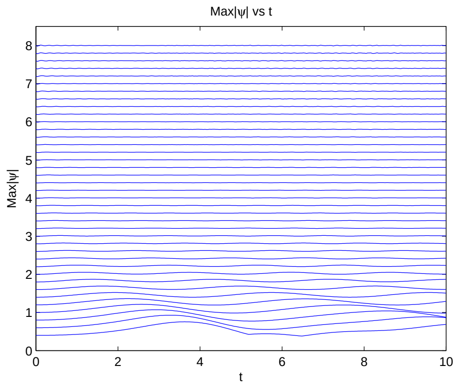

(a) Max $|\psi|$ propagation with time. The soliton width range $(0.125-2.5)$. Each line represents different widths. $\Delta x = 2L/N$, $L = 10$, $N = 2^{10}$.

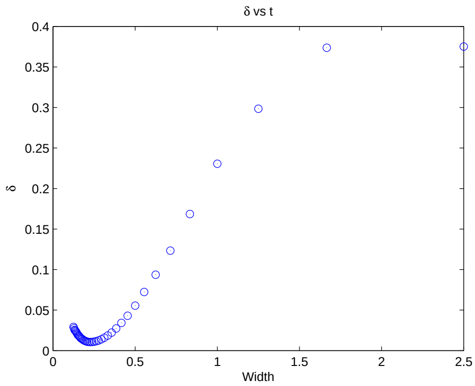

(b) Max $|\psi|$ varying range (δ) vs the width of soliton

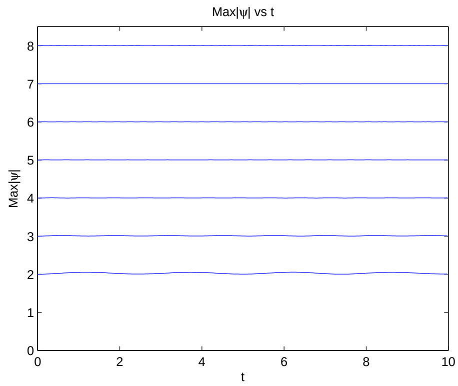

(c) Improved accuarcy of Max $|\psi|$ propagation with time. The soliton width range $(0.125-0.5)$. Each line represents different widths. $\Delta x = 2L/N$, $L = 10$, $N = 2^{12}$.

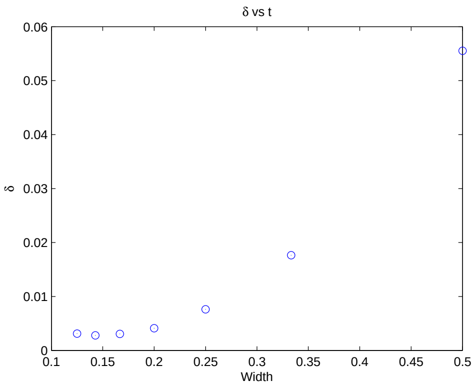

(d) Improved accuarcy of Max $|\psi|$ varying range (δ) vs the width of soliton

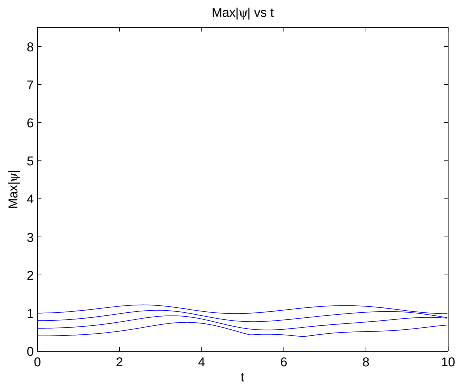

(e) Improved accuarcy of Max $|\psi|$ propagation with time. The soliton width range $(1-2.5)$. Each line represents different widths. $\Delta x = 2L/N$, $L = 10$, $N = 2^{12}$.

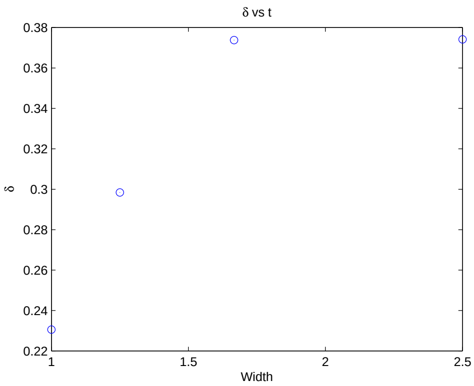

(f) Improved accuarcy of Max $|\psi|$ varying range (δ) vs the width of soliton

Figure 2.3: Time-independent periodic potential, $W(x,t) = -\cos(k_0 x)$, $k_0 = 0.5$, $k_{mod} = 0$.

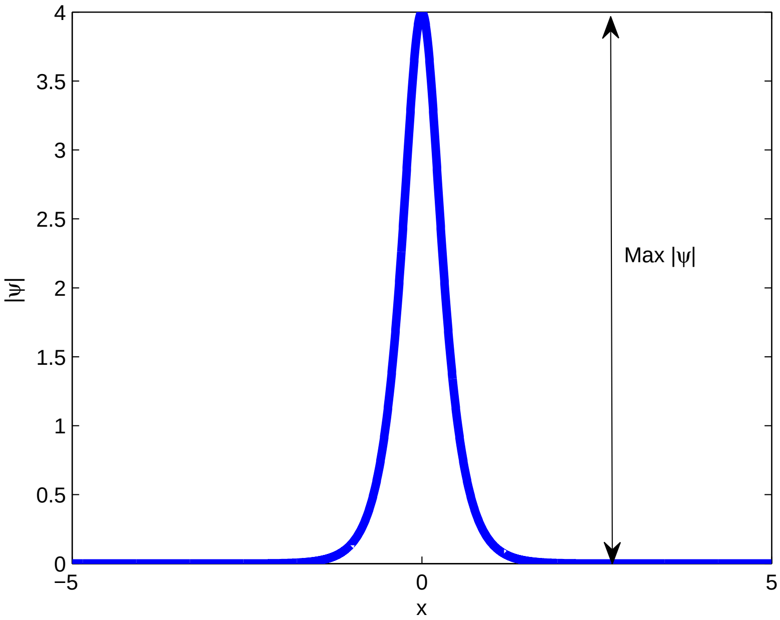

Figure 2.4: Exact lowest order stationary soliton solution of the nonlinear Schrödinger equation. $A = 1/w = \sqrt{2\alpha} = 4$

the stationary solution with the exact soliton solution found for $W(x,t) = 0$:

$$u_{ans} = \sqrt{2\alpha}\,\mathrm{sech}\left[\sqrt{2\alpha}\,(x - x_0)\right] = A\mathrm{sech}\left(\frac{x - x_0}{w}\right) \tag{2.4}$$

where α is a real parameter, corresponding to the chemical potential in a BECs context. A, x_0 and w represent the amplitude, centre of mass and width respectively. So we have $A = 1/w = \sqrt{2\alpha}$.

2.2.3 Numerical propagation

We use that the NLSE soliton as an initial condition for the evolution method. For $W(x\,,t) \neq 0$ it is generally not possible to find exact solutions to the NLSE (2.1). Exact solutions of the NLSE have been investigated extensively by many scientists. Numerical methods are typically needed to find solutions when the potential is present.

A numerical method commonly used is the split-step Fourier method introduced by Hasegawa and Tappert. [31]. This numerical method separates the linear and nonlinear, then solve them sequentially. The outline of the split-step Fourier method algorithm follow:

1. Solve the linear operator equation

$$i\frac{\partial\psi}{\partial t}+\frac{1}{2}\frac{\partial^2\psi}{\partial x^2}=0 \tag{2.5}$$

Taking a Fourier transformation, we have

$$i\frac{d\mathcal{F}}{dt}-\frac{1}{2}k^2\mathcal{F}=0 \tag{2.6}$$

Where $\mathcal{F}=\int_{-\infty}^{\infty}\psi e^{-jx\Delta t}dt$, solve equation (2.6), we have

$$F_l=\mathcal{F}_0 e^{-ik^2\Delta t/2} \tag{2.7}$$

When we take an inverse Fourier transformation, we should obtain

$$\psi_0=\frac{1}{2\pi}\int_{-\infty}^{\infty}\mathcal{F}e^{jx\Delta t}dx$$

and $\mathcal{F}_0$ is a constant.

2. Solve the nonlinear operator equation

$$i\frac{d\psi}{dt}-W(x,t)\psi+|\psi|^2\psi=0 \tag{2.8}$$

$|\psi|^2$ is a constant N, thus:

$$i\frac{d\psi}{dt}-W(x,t)\psi+N\psi=0 \tag{2.9}$$

The solution of Equation(2.9) is $\psi=\psi_0 e^{i[N-W(x,t)]\Delta t}$, where ψ_0 is the solution of the linear part, $\psi_0=\frac{1}{2\pi}\int_{-\infty}^{\infty}\mathcal{F}e^{jx\Delta t}dx$.

These two steps are iterated to propagate the field ψ forward in time. To ensure a numerically stable propagation we require the condition [32]

$$\Delta t\leqslant(\Delta x)^2\,, \tag{2.10}$$

to hold. Here Δt is the time step and Δx is spatial step size.

2.2.4 Variational approach

In the variational approach, we focus on the centre of mass of the soliton. In doing so we treat the soliton as if it were a particle. It is necessary to assume that both the amplitude and the width of soliton are constants. Numerically, the variational approach is a simpler method to solve our problem. The approximate solutions are obtained for the evolution during propagation of the centre of mass. This allows the reduction of the complexity of the PDE problem to one of solving an ODE for the center of mass of the soliton. The solutions show very good agreement with results from solving the full PDE system numerically. It is often desirable to obtain some physical insight into the problem that numerical schemes cannot provide, and thus approximate solutions deduced by such methods as a variational approach become important.

The problem of the nonlinear Schrödinger equation is reformulated as a variational problem (see Ref. [33] for a similar derivation) via

$$\delta \iint \mathcal{L}\, dx\, dt = 0\,,$$

with the Lagrangian density:

$$\mathcal{L} = \frac{i}{2}(\psi\psi_t^* - \psi^*\psi_t) + \frac{1}{2}|\psi_x|^2 - W(x,t)|\psi|^2 + \frac{1}{2}|\psi|^4. \tag{2.11}$$

A general variational ansatz is [33]:

$$\psi_{ans} = A(t)\,\mathrm{sech}\left(\frac{x - x_0(t)}{w(t)}\right) e^{iv(t)(x-x_0(t))+i\beta(t)(x-x_0(t))^2}\,, \tag{2.12}$$

however we significantly simplify the analysis by assuming time-independence of the amplitude, $A(t) = A$, and width $w(t) = w$, and a zero chirp, $\beta(t) = 0$, i.e. that the soliton is "particle-like". This assumption is reasonable when the external driving frequency is far from any internal modes of the soliton [33]. Our variational parameters are thus reduced to only the position of the soliton's centre-of-mass $x_0(t)$ and the soliton centre-of-mass velocity $v(t) = \dot{x}_0$.

Substituting this ansatz into the Lagrangian density(2.11), there is an effective Lagrangian density, $\mathcal{L}_{\mathrm{eff}} = \mathcal{L}[\psi_{ans}]$:

$$\begin{aligned}\mathcal{L}_{\mathrm{eff}} &= |A|^2[-v\frac{d(x_0(t))}{dt} + (x - x_0(t))\frac{dv}{dt}]\mathrm{sech}^2\left(\frac{x - x_0(t)}{w}\right)\\ &+ \frac{1}{2}|A|^2[\frac{1}{w^2}\tanh^2\left(\frac{x - x_0(t)}{w}\right) + v^2]\mathrm{sech}^2\left(\frac{x - x_0(t)}{w}\right)\\ &+ |A|^2 W(x,t)\mathrm{sech}^2\left(\frac{x - x_0(t)}{w}\right) + \frac{1}{2}|A|^4\mathrm{sech}^4\left(\frac{x - x_0(t)}{w}\right).\end{aligned} \tag{2.13}$$

Next we integrate the effective Lagrangian density $\mathcal{L}_{\text{eff}}$ (2.13)to obtain an effective Lagrangian:

$$\begin{aligned} L_{\text{eff}} &= \int_{-\infty}^{\infty} \mathcal{L}_{\text{eff}}\, dx \\ &= -2|A|^2 wv \frac{d(x_0(t))}{dt} + \frac{|A|^2(1+3v^2w^2)}{3w} + \frac{2}{3}|A|^4 w \\ &+ \int_{-\infty}^{\infty} |A|^2 W(x,t) \text{sech}^2\left(\frac{x-x_0(t)}{w}\right) dx \end{aligned} \tag{2.14}$$

Applying the Euler-Lagrange equations:

$$\frac{d}{dt}\frac{\partial L_{\text{eff}}}{\partial \dot{q}_j} = \frac{\partial L_{\text{eff}}}{\partial q_j} \tag{2.15}$$

where q_j are the parameters x_0 and v, we derive the following equations:

$$\dot{x_0}(t) = v, \tag{2.16}$$

$$\ddot{x_0}(t) = -\frac{1}{2w}\frac{\partial}{\partial x_0}\int_{-\infty}^{\infty} W(x,t)\,\text{sech}^2\left(\frac{x-x_0}{w}\right) dx. \tag{2.17}$$

We use this result in all our following investigations of the system dynamics.

2.3 Results

We discuss soliton dynamics in both time-independent and time-dependent potentials. We start with the simpler time-independent parabolic and periodic potentials before analysing the frequency modulated potential (2.2). The variational approach is used in each case and compared with the solution obtained by solving (2.1).

2.3.1 Time-independent parabolic potential.

We start with the simple case of a time-independent parabolic potential

$$W(x,t) = \frac{1}{2}\omega_0^2 x^2\,. \tag{2.18}$$

Substituting equation (2.18) into equation (2.17), we have:

$$\ddot{x}_0 + \omega_0^2 x_0 = 0\,. \tag{2.19}$$

Equation (2.18) shows that the soliton is moving in a harmonic potential. The initial condition is the NLSE soliton (2.4). There are small changes of Max$|\psi|$ in Fig 2.5. Figure 2.6(a) shows a plot of the potential. As the energy is conserved the particle-like soliton is trapped in the potential and exhibits oscillatory motion.

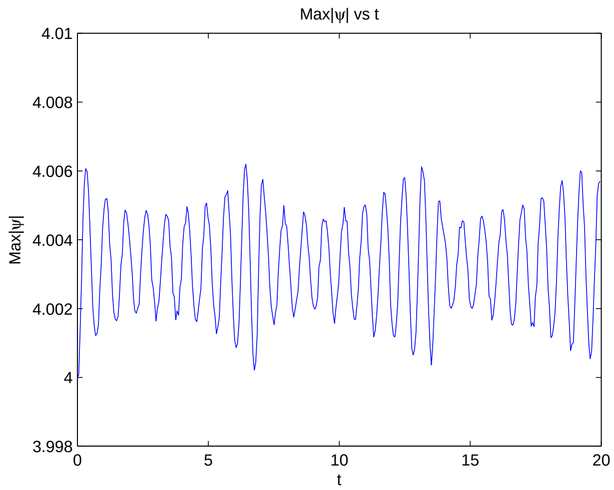

Figure 2.5: Max $|\psi|$ propagation with time in the parabolic potential. The varying of Max $|\psi|$ is small. The soliton width ($w = 0.25$).

The centre-of-mass of a soliton with initial position $x_0(0) = 2$ released from rest is described by

$$x_0(t) = 2\cos(\omega_0\, t)\ . \tag{2.20}$$

Figure 2.6(b) shows the time evolution of the centre-of-mass of the soliton described by the variational solution (2.20) with ($w = 0.25$). We compared PDE and ODE results in figure 2.6 (b) and (d). Figure 2.6(c) is a contour plot of the intensity of the soliton overlayed with the variational solution (white). It is clear to see these two methods results are in a good agreement from solving the equation (2.21)

$$\text{Error} \;=\; \frac{\displaystyle\int_{-\infty}^{\infty} x|\psi|^2 dx}{\displaystyle\int_{-\infty}^{\infty} |\psi|^2 dx} - x_0(t). \tag{2.21}$$

This simple case suggests that the approximation in ODE system is a useful tool for analysing dynamics. In particular, we see that the maximum error is 7×10^{-4}, remarkably almost two orders of magnitude less than the spatial resolution of the soliton in the PDE model (4×10^{-2}).

2.3.2 Time-independent periodic potential.

At this stage, we introduced a time-independent periodic potential in equation (2.22), which only causes a spatial displacement of potential,

$$W(x,t) = -\cos(k_0 x) \tag{2.22}$$

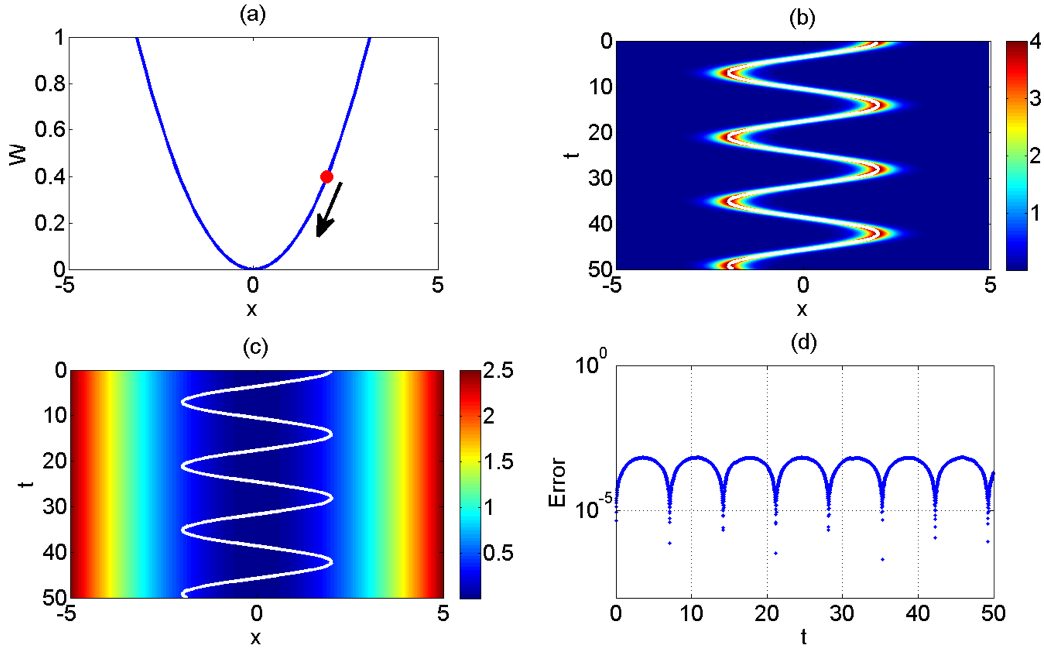

Figure 2.6: Dynamics in a parabolic potential with $\omega_0 = \sqrt{0.2}$, $x_0 = 2$ and $\dot{x}_0(0) = 0$. Parameters: $L = 5$, $N = 2^8$, $\Delta x = 2L/N$, $\Delta t = 0.0015$,the actual value of the maximum error: 6.7699×10^{-4}. The soliton in a parabolic potential in (a), (c) and the comparison results from ODE (the central white line in figure (b) and (c)) and PDE methods in (b),(d). We can see the differences in position between PDE and ODE results in figure (d).

A plot of the potential is shown in Figure 2.8(a). Substituting equation (2.22) into equation (2.17), we have:

$$\ddot{x_0} + \frac{\pi}{2} w k_0^2 \sin\left(k_0 x_0(t)\right) \operatorname{csch}\left(\frac{w\pi k_0}{2}\right) = 0 \tag{2.23}$$

The initial condition is the NLSE soliton (Fig. 2.7). There are small variations of Max$|\psi|$. Figure 2.8(b) shows a contour plot of the effective potential and the time evolution of the centre-of-mass with initial displacement $x_0(0) = 2$ and velocity $\dot{x}_0(0) = 0$. Since energy is conserved, a soliton initially at rest and with initial position $x_0(0) = 2$ will at first roll down the potential and then up the potential until reaching $x_0 = -2$. At this point the soliton slides back down then up the potential until reaching $x_0 = 2$. The particle-like soliton is trapped in the potential and executes a periodic trajectory as it evolves in time.

Figure 2.8(c) displays a contour plot of the intensity of the soliton obtained by solving (2.1). The difference between this and the variational solution is illustrated in Figure 2.8(d). Once again, there is good agreement between the two methods

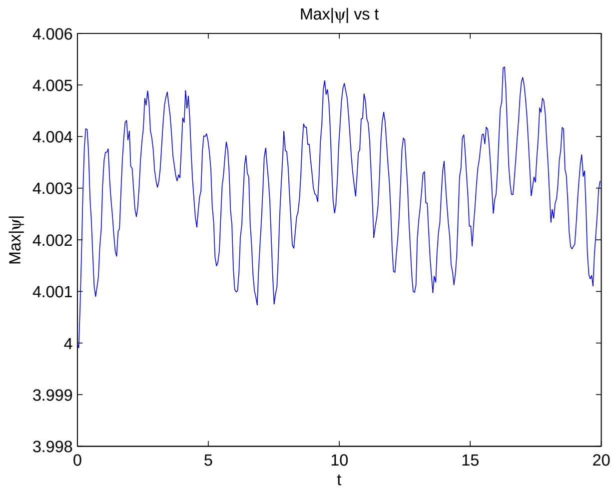

Figure 2.7: Max $|\psi|$ propagation with time in a periodic potential. The soliton width ($w = 0.25$). The varying of Max $|\psi|$ is small. $W(x,t) = -\cos\left[k_0 + k_{mod}\sin(\eta t)\right]x$, $k_0 = 0.5$, $k_{mod} = 0$, and $x_0 = 2$.

with the largest differences being at the turning points. Again we see very good agreement between the position of the soliton predicted by the ODE model, compared with the PDE results. The maximum discrepancy is again 7×10^{-4}, much less than our PDE spatial resolution of 8×10^{-2}.

For soliton dynamics in the vicinity of the minimum of the potential, where $x_0(t)$ is small, by linearising (2.23) we obtain $\ddot{x}_0 + \Omega^2 x_0 = 0$ where

$$\Omega^2 = \frac{\pi}{2} w k_0^3 \operatorname{csch}\left(\frac{w\pi k_0}{2}\right), \tag{2.24}$$

which represents simple harmonic motion with natural frequency Ω. Note that Ω does not depend on x_0, whereas in general the eigenfrequency of a nonlinear oscillator does depend on the amplitude of the oscillations.

2.4 Conclusion

Our research model and methods have been presented in this chapter. By study soliton in time-independent potentials, we find the variational approach is a simpler and more effective method than numerical propagation. Therefore, we will study soliton in time-dependent potentials by using variational approach in the following chapter.

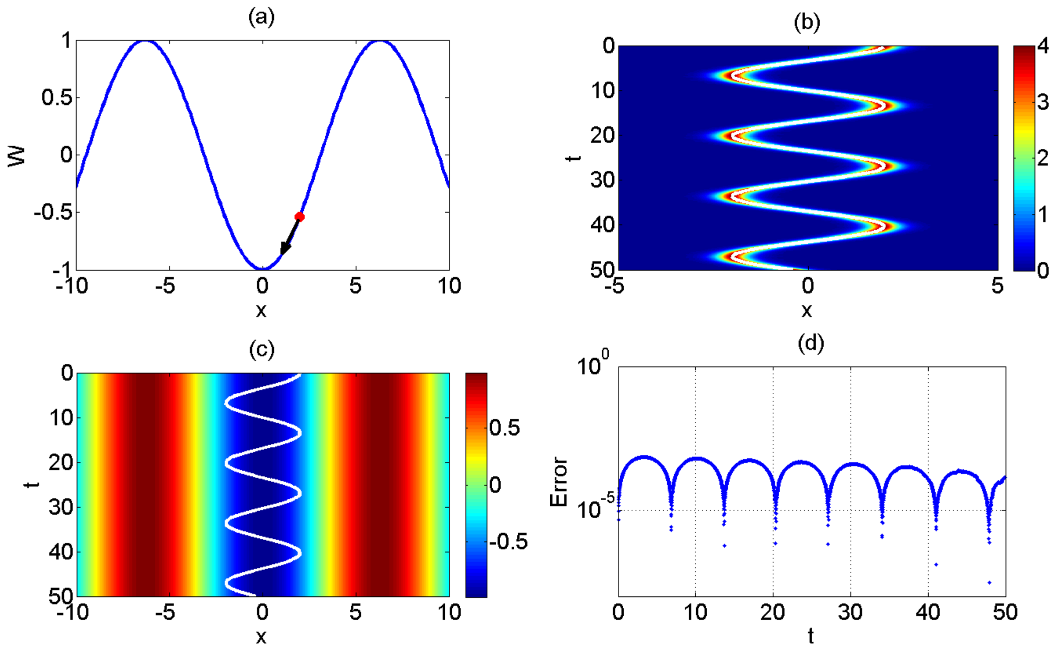

Figure 2.8: Dynamics in a time-independent periodic potential with $k_0 = 0.5$, $x_0 = 2$ and $\dot{x}_0(0) = 0$. Parameters: $L = 10$, $N = 2^8$, $\Delta x = 2L/N$, $\Delta t = 0.0015$, the actual value of the maximum error: 6.8701×10^{-4}. Comparison between the variational solution (b) and that of the numerical solution (c) is shown in (d).

Chapter 3

Time-dependent frequency-modulated potential.

In the previous chapter, we introduced our research model and methods. From the simple time-independent cases results, we demonstrated our variational approach is an effective tool. Thus, we continue our study in the full time-dependent potential by using the variational method model, which simplifies the complicated problem. We also use tools from the study of dynamical systems: the Poincaré section.

3.1 Time-dependent potential.

We analyse the soliton dynamics in a time-dependent frequency-modulated periodic potential given by equation (2.2)

$$W(x,t) = -\cos\left[k(t)x\right] , \quad k(t) = k_0 + k_{mod}\sin(\eta t) .$$

In this case, we consider the periodic potential with a time dependent spatial frequency $k(t)$. Substituting equation (2.2) into the general variational equation (2.17), we have:

$$\ddot{x_0} + \frac{\pi}{2} w k(t)^2 \sin\left[k(t)x_0(t)\right] \operatorname{csch}\left(\frac{w\pi k(t)}{2}\right) = 0. \tag{3.1}$$

As the potential $W(x,t)$ now is changing with time, energy is not conserved in the system and the soliton may undergo particle-like driving. The resultant dynamics depend on the initial position of the soliton relative to the time-varying potential, and on the parameters of the potential itself. First we consider the influence of the initial conditions in the case of a weak non-resonant potential i.e. a small amplitude potential with an oscillation frequency far from any internal modes of the soliton, or characteristic frequencies of the time-independent potential. To this end we take $k_0 = 0.5$, $k_{mod} = 0.05$ and $\eta = 0.1$, and we study this case in section 3.2. We find different classes of motions depending on initial conditions. In section 3.3, we consider the resonant case with parameters: $k_0 = 0.5$, $k_{mod} = 0.05$ and $\eta = 1$, and we find parametric driving when driving frequency is twice the potential frequency. In section 3.4 and 3.5, briefly we discuss results of soliton dynamics in an asymmetric potential and a damped time dependent potential.

3.2 Non-resonance dynamics

There are two types of motion occurring when we study non-resonant dynamics, which are depended on initial conditions.

3.2.1 Oscillation in the minima of the potential.

The soliton obtains the energy from the squeezing of the potential, to move a higher position in the potential well. It slides back to the minima when the potential expands. Because the squeezing produces a force and the direction of this force is perpendicular to the contact surface of soliton and potential, the soliton is moved by this force. However, there is no contact when the potential expends, so 'gravity' pulls the soliton back down to the minima. Then it is trapped periodically in Fig.3.1 (a). Figure 3.1 (b) shows the differences in position between the results from numerically solving PDE and variational approach by solving equation (2.21). These differences are below the spatial resolution of the PDE so within the accuracy of our simulations we see perfect agreement. Fig.3.2 shows the comparison of the results from the numerical method and the variational approach (the centre white line). The results are in a good agreement.

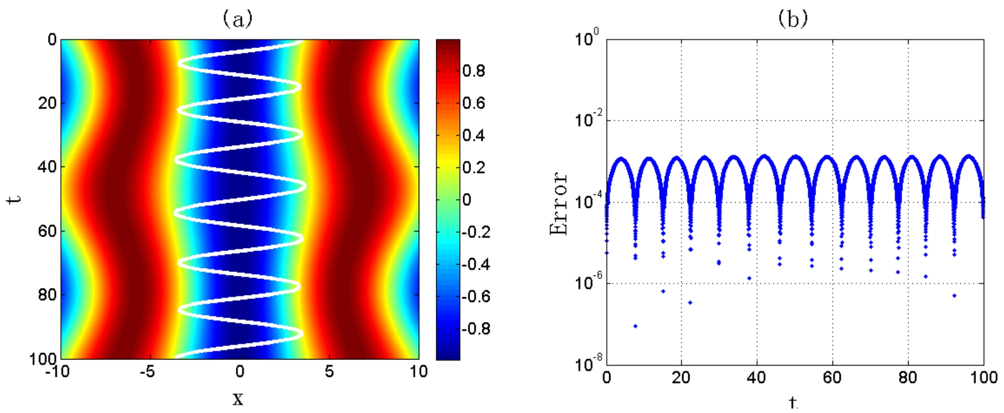

Figure 3.1: (a) shows the comparison of results from numerical method and variational approach (the central white line in figure (a)), the potential $W(x,t) = -\cos[k_0 + k_{mod}\sin(\eta t)]x$. The initial condition are: $x_0 = 3.5$, $k_0 = 0.5$, $k_{mod} = 0.05$, $\eta = 0.1$. The particle-like soliton is trapped in the blue area which presents the lower density of the potential. (red and blue correspond to the maxima and minima of the potential respectively) In figure 3.1 (b), we can see the differences in position between PDE and ODE results.

3.2.2 Motion between potential wells.

The soliton moves between potential wells depending on its initial conditions. We set an initial position $x_0(t) = 6$, because this position is almost the highest position of the potential well. In this circumstance, the soliton has enough energy to jump to the adjacent potential well and is trapped for a while. In section 3.1, we considered a soliton in a time-dependent frequency-modulated periodic potential.

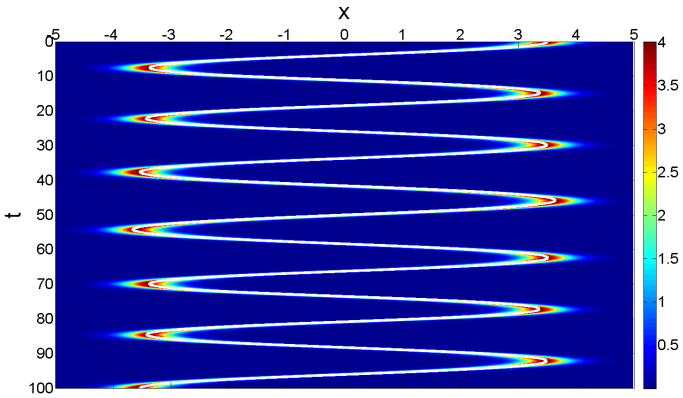

Figure 3.2: Comparison the results of numerical method and variational approach (the central white line) in the potential $W(x,t) = -\cos[k_0 + k_{mod}\sin(\eta t)]x$. The initial condition are: $x_0 = 3.5$, $k_0 = 0.5$, $k_{mod} = 0.05$, $\eta = 0.1$.

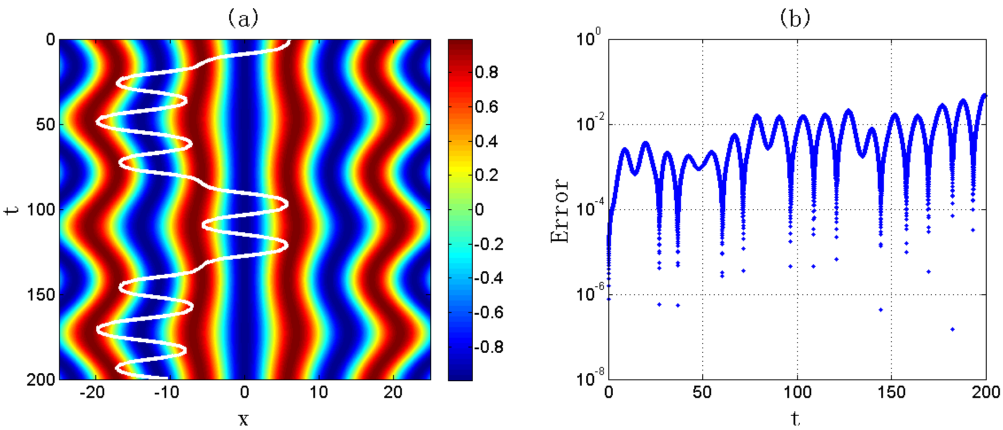

Figure 3.3: Jumping case with potential and the initial conditions are: $x_0 = 6$, $k_0 = 0.5$, $k_{mod} = 0.05$, $\eta = 0.1$. In figure (a), the central white line presents the result from variational approach. In figure (b), we can see the differences in position between PDE and ODE results.

The squeezing of the potential well provides the energy to the soliton which moves back to its original well. Thus, we could conclude a certain frequency of squeezing providing enough energy to allow the soliton to move between potential wells.

It is clear that the potential is varying more intensely far from the centre in figure 3.3 (a). Figure 3.3 (b) provides the results of differences in position between PDE and ODE and the trend of these differences is increasing with time. Fig.3.4 shows the comparison of the results from the numerical method and the variational approach (the centre white line). The results are in a good agreement over the time domain $0 \leqslant t \leqslant 200$.

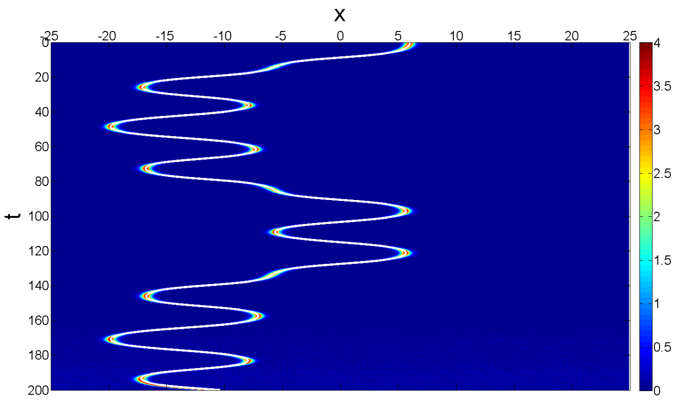

Figure 3.4: Comparison the results of numerically solving PDE and variational approach (the central white line) in the potential $W(x,t) = -\cos[k_0 + k_{mod}\sin(\eta t)]x$. The initial condition are: $x_0 = 6$, $k_0 = 0.5$, $k_{mod} = 0.05$, $\eta = 0.1$.

3.2.3 Initial condition

We focus on a small range of initial conditions, for instance, $-6 \leqslant x_0 \leqslant 6$ between two maxima of the potential in a short time period, and study the finial position x and velocity v. The results in Fig. 3.5 show that the corresponding finial coordinate (x, v) for each initial condition (Fig.3.5 left shows the finial positions and Fig. 3.5 right represents the corresponding finial velocities). For instance, when the initial condition is $x = -5, v = -3$, the finial position (from the left figure) and final velocity (from the right figure) are -2393.9 and -2.0162, respectively. There is a symmetry about the coordinate centre $(0, 0)$ both for final x and final v. Also, it is demonstrated that the soliton is trapped with initial conditions x and v centred $(0, 0)$. However, initially high speed or a starting position near the maximum of the potential results in high final speed and large displacement from the origin.

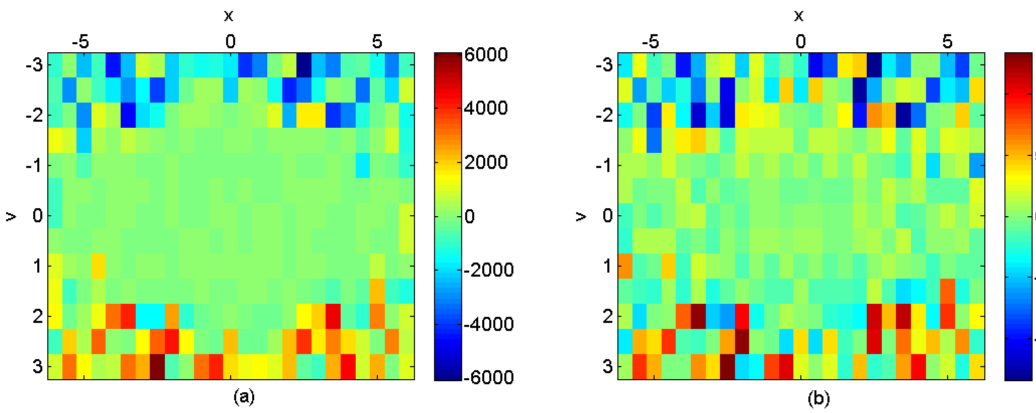

Figure 3.5: A couple of value figures which shows the final positions in (a) and final velocities in (b) for different initial conditions at a time equal to 10 times the force period. Parameters: $-6 \leqslant x_0 \leqslant 6, -3 \leqslant v_0 \leqslant 3, k_0 = 0.5, k_{mod} = 0.05, \eta = 0.1, 0 \leqslant t \leqslant 20\pi/\eta$.

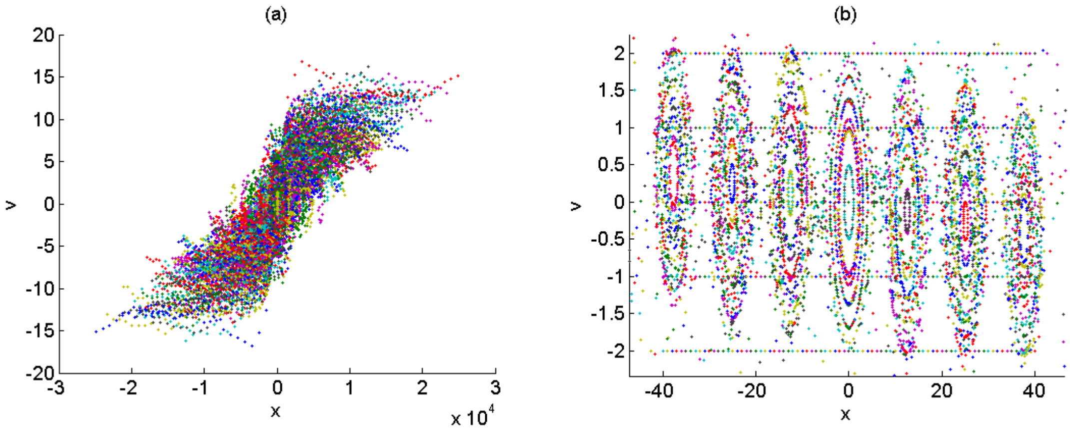

Figure 3.6: Poincare map created by sampling 1000 ODE solutions from $t = 0$ to $t = 2000$ every $t = 2\pi/\eta$. Quasi-periodic trapped solutions are evident as circles, chaotic motion appears as disconnected dots. Parameters of time-dependent potential: $-40 \leqslant x_0 \leqslant 40$, $-4 \leqslant v_0 \leqslant 4$, $k_0 = 0.5$, $k_{mod} = 0.05$ and $\eta = 0.1$.

Poincaré section

To better understand the influence of the initial conditions we can represent the dynamics on a Poincaré map, sampled at the frequency of the potential. We see in Fig. 3.6 the existence of quasi-periodic motion about the minima near the centre, and also a chaotic layer connecting the maxima of the potential. Moving further from the centre the regions of quasi-periodic motion grow smaller, to be replaced ultimately by an extended chaotic layer. We notice some interesting properties of the trajectories in this layer, in particular the appearance of quasi-ballistic motion far from the centre. Also, several elliptical orbits appear in Fig. 3.6, which means that the soliton is trapped by the potential wells. We thus see that in general the soliton experiences chaotic jumps and oscillations close to the centre but ultimately escapes, propagating away at a velocity determined by the characteristics of the potential.

Histogram

In statistics, a histogram is a series of rectangles of equal base and whose heights represent the probability distribution of data [34]. By using this method, we can estimate the probability density function of the time series. However, it should be aware that this histogram method ignores the temporal ordering information.

In our research, there are two aspects considered distinguished by the initial conditions. One of these is that a certain initial condition is fixed for both x_0 and v_0. We collected statistics of the velocities for t from 0 to 10000. Also, figure 3.7 suggests that a large number of velocities are high (around $v = 9$). We obtained more results for different initial positions and velocities (Fig. 3.8-3.10). We find

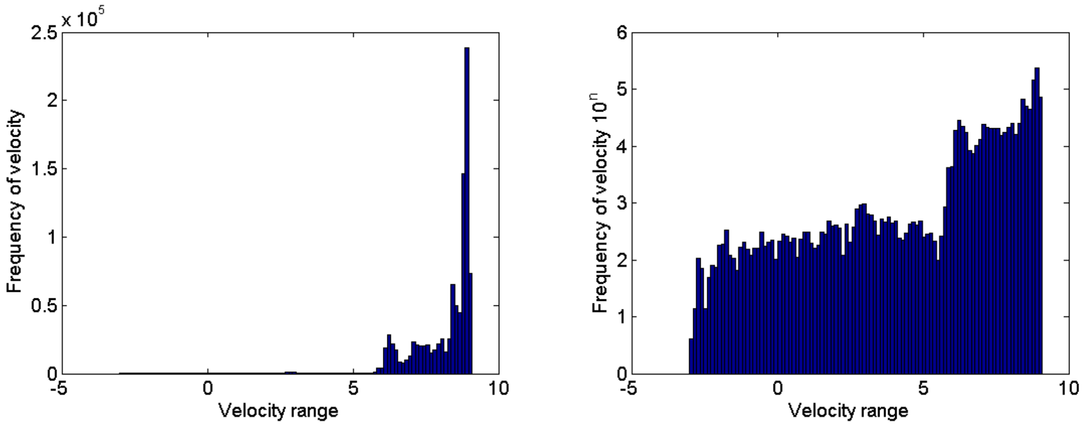

Figure 3.7: A histogram of velocities. (a) shows the velocity frequencies in 100 intervals within velocity range. The vertical axis of (b) is logarithmic (base 10) scale of the vertical axis in figure (a) Parameters: $x_0 = 6, v_0 = 3, k_0 = 0.5, k_{mod} = 0.05, \eta = 0.1, 0 \leqslant t \leqslant 10000$.

that soliton dynamics is depending on the initial condition. The soliton was moving from approximately the maximum of the potential with zero speed. Thus, the soliton gained enough energy, which is provided by the squeezing potential well, to reach high velocity.

Another set of initial conditions for both x_0 and v_0 is shown in Fig 3.11 and 3.12. In figure 3.11, we use $-40 \leqslant x_0 \leqslant -40, -4 \leqslant v_0 \leqslant -4$ as initial conditions. The histogram plot is a representation of frequencies of velocities under different initial conditions (the number of velocities is 22599), shown as adjacent rectangles in equal interval. Also, we focus on a smaller range of initial conditions $-20 \leqslant x_0 \leqslant -20, -2 \leqslant v_0 \leqslant -2$, but for a longer time period $t = 10000$ in Fig 3.12. We find that the large frequencies of velocities locate around low speed and it is a symmetrical histogram plot.

3.3 Parametric resonance

The energy of oscillations is provided by periodically changing the spatial period with time, i.e. varying a parameter of the system (the spatial period). Parametric resonance occurs when the spatial period is varied at a frequency which is twice the frequency of the trapping potential. To remain within our particle-like approximation for the soliton we restrict our attention to resonances between the oscillation frequency and spatial frequency of the potential (rather than a resonance with the soliton internal modes [33]). In particular, guided by the results of [27] we consider the possibility of parametric driving of the soliton centre-of-mass. Here too, the

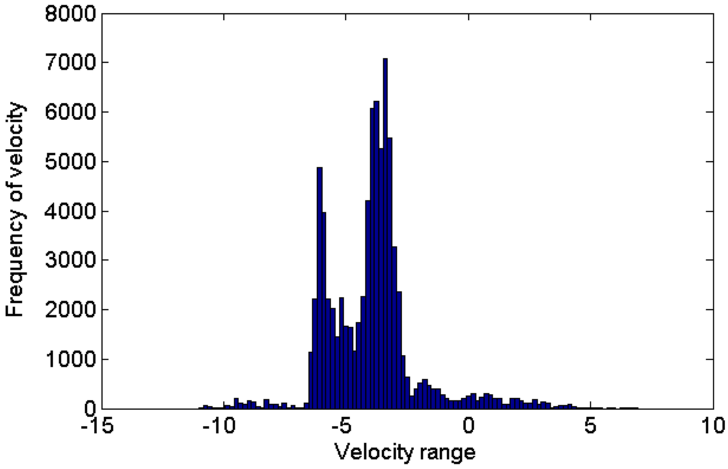

Figure 3.8: A histogram of velocities. The velocity frequencies in 100 intervals within velocity range. Parameters: $k_0 = 0.5, k_{mod} = 0.05, \eta = 0.1, x_0 = 2, v_0 = 4, 0 \leqslant t \leqslant 50000$.

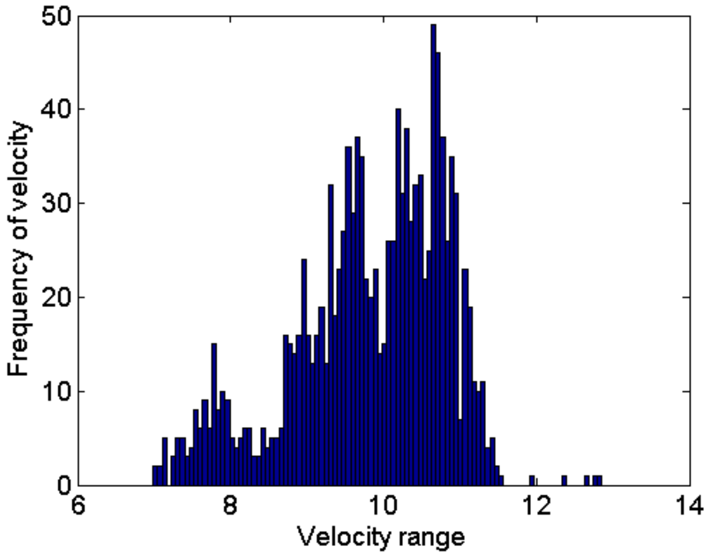

Figure 3.9: A histogram of velocities. The velocity frequencies in 100 intervals within velocity range. Parameters: $k_0 = 0.5, k_{mod} = 0.05, \eta = 0.1, x_0 = 2, v_0 = 10, 0 \leqslant t \leqslant 80000$.

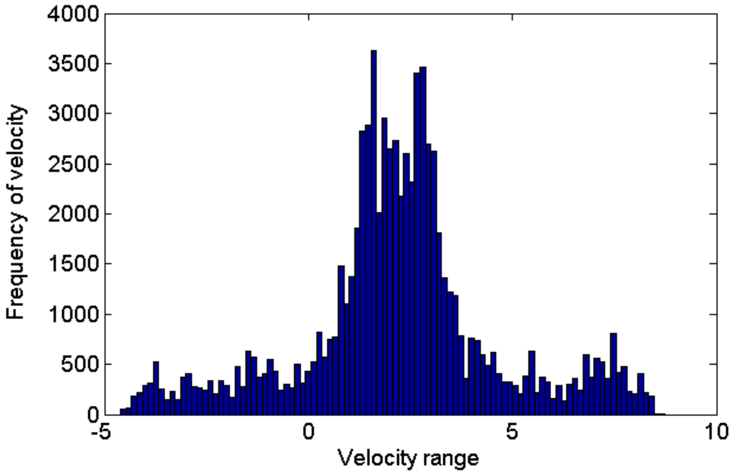

Figure 3.10: A histogram of velocities. The velocity frequencies in 100 intervals within velocity range. Parameters: $k_0 = 0.5, k_{mod} = 0.05, \eta = 0.1, x_0 = 4, v_0 = 2, 0 \leqslant t \leqslant 50000$.

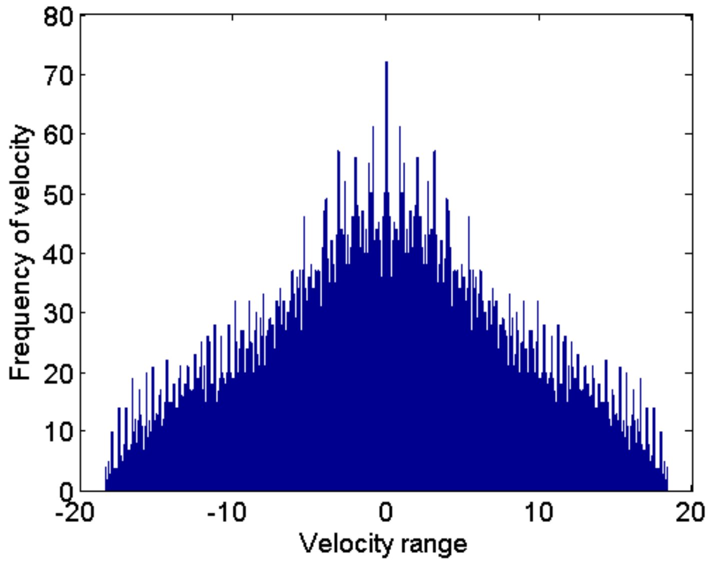

Figure 3.11: A histogram of velocities. Parameters: $k_0 = 0.5, k_{mod} = 0.05, \eta = 0.1, -40 \leqslant x_0 \leqslant 40, -4 \leqslant v_0 \leqslant 4$.

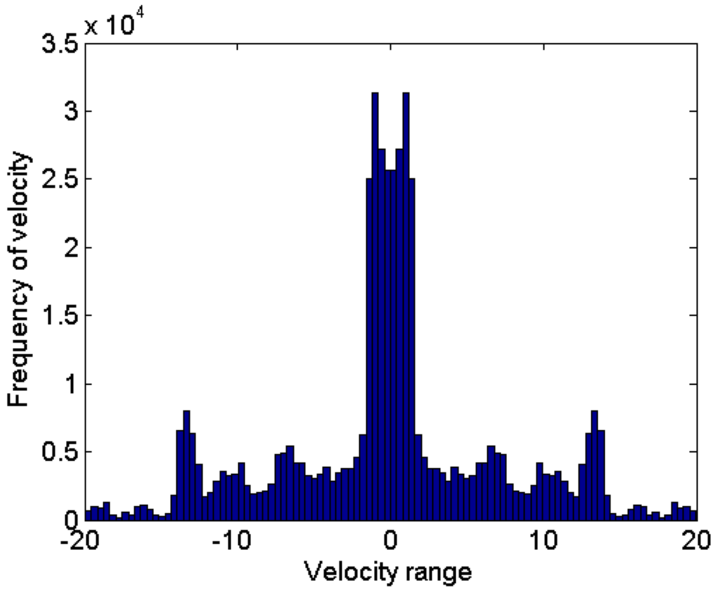

Figure 3.12: A histogram of velocities. Parameters: $k_0 = 0.5, k_{mod} = 0.05, \eta = 0.1, -10 \leqslant x_0 \leqslant 10, -2 \leqslant v_0 \leqslant 2, 0 \leqslant t \leqslant 10000$.

effect of a frequency-modulated potential can be modelled by ODE (3.1). For small x_0, linearising (3.1), and noting that $k_{mod} \ll k_0$, leads to

$$\ddot{x}_0 + \Omega^2 \left(1 + \left(\frac{3k_{mod}}{k_0} - \frac{w\pi}{2}\coth(w\pi k_0/2)\right)\sin(\eta t)\right) x_0 = 0\,. \tag{3.2}$$

where $\Omega^2 = \pi w k_0^3 \text{csch}(w\pi k_0/2)/2$. Equation (3.2) is the well-known Mathieu equation which exhibits parametric resonance when $\eta = 2\Omega$ [35]. This condition is approximately satisfied for the parameters used in generating Figure 3.13. At resonance, starting with a small displacement from the centre, according to (3.2) the amplitude of the oscillations about the centre will increase without bound. Clearly Figure 3.13 does not sustain this. The reason is that when x_0 becomes large, the dynamics are governed by (3.1) rather than (3.2). The effect of nonlinearity is to limit the amplitude of oscillations by shifting the eigenfrequency out of resonance [36]. This leads to the decay of the amplitude of the position of the soliton. When x_0 is sufficiently small, the eigenfrequency is back in resonance and the amplitude begins to grow again.

3.3.1 Poincaré section and histogram

We explore the dependence of the parametric resonance on the initial conditions. We represent the different resulting dynamics on a Poincaré map. Figure 3.14 shows that the soliton dynamics is a quasi-periodic motion within the minima near the centre, and also a chaotic layer connecting the maxima of the potential. This quasi-periodic motion is similar to the regular motion (in section 3.2.1). Furthermore,

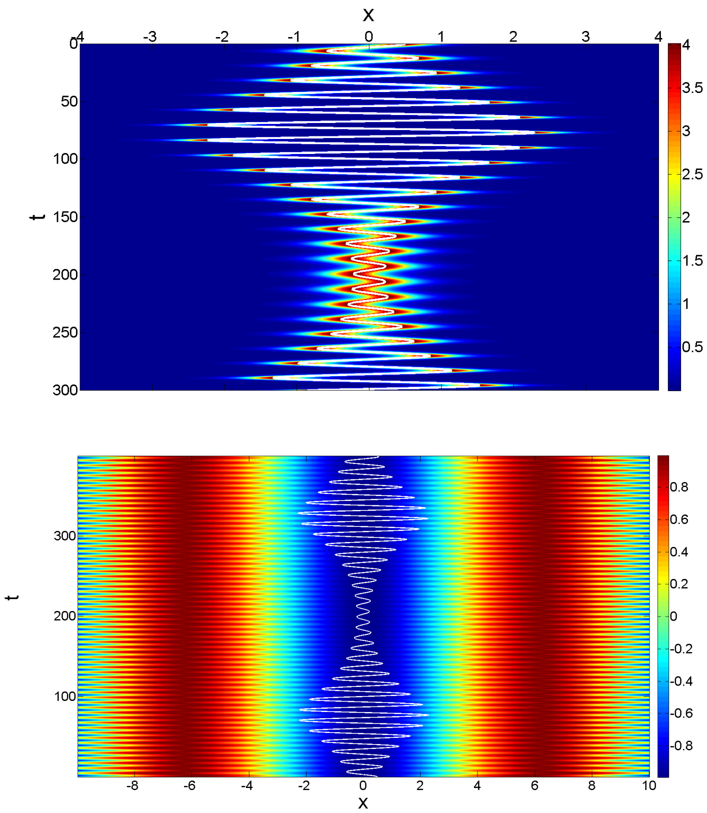

Figure 3.13: The upper figure shows that the comparison of numerical method and variational approach (the central white line). The lower figure illustrates the trajectory of the particle. The initial condition is $x_0 = 0.5$, $k_0 = 0.5$, $k_{mod} = 0.05$, $\eta = 1$ and $\Omega = 0.498398$.

there is a symmetry about the coordinate centre $(0, 0)$ both for position x and velocity v. Also, this symmetry character is shown in Fig.3.15.

3.4 Asymmetric potential

Another interesting case we studied, is the soliton in an asymmetric potential:

$$W(x,t) = -\cos\left(k(t)x\right) \ , \quad k(t) = k_0 + k_{mod}\left(\sin(\eta t) \pm 0.3\sin(2\eta t)\right) \ , \qquad (3.3)$$

In Fig.3.16 (a), we present the regular motion potential, which is symmetric. But figure (b) and figure (c) are asymmetric, which are due to $k_{mod}\left(\sin(\eta t) \pm 0.3\sin(2\eta t)\right)$ respectively. Fig. 3.17 and 3.18 exhibit that the soliton dynamics is quasi-periodic motion near the centre and there is a chaotic layer as well. For the purpose of better understanding the asymmetric potentials, we provide a comparison of position x and velocity v via Poincaré sections and histograms in Fig. 3.19-3.21. The remarkable similarity, for instance, is that the quasi-periodic motion exists in both

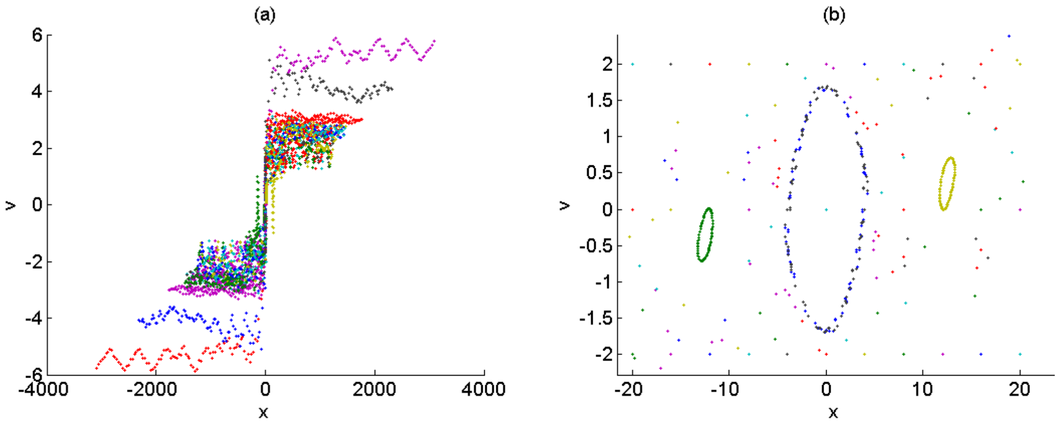

Figure 3.14: Poincare map created from $t = 0$ to $t = 600$ every $t = 2\pi/\eta$. Quasi-periodic trapped solutions are evident as circles, chaotic motion appears as disconnected dots. Parameters of time-dependent potential: $-20 \leqslant x_0 \leqslant 20$, $-2 \leqslant v_0 \leqslant 2$, $k_0 = 0.5$, $k_{mod} = 0.05$ and $\eta = 1$.

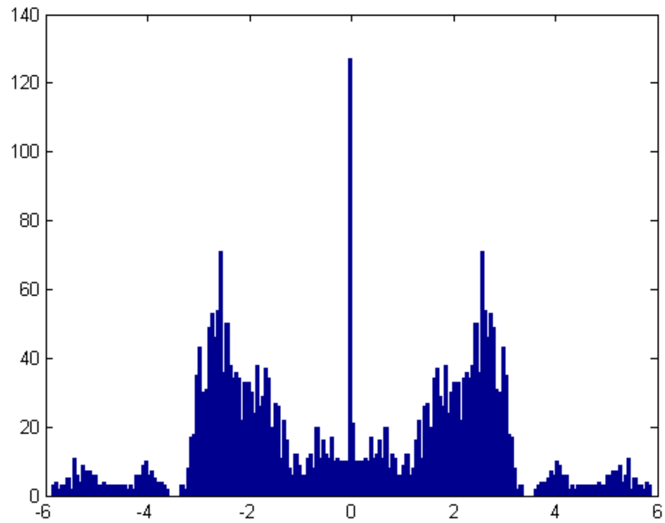

Figure 3.15: A histogram of a set of initial conditions for velocities. Parameters: $k_0 = 0.5, k_{mod} = 0.05, \eta = 1, -20 \leqslant x_0 \leqslant 20, -2 \leqslant v_0 \leqslant 2, 0 \leqslant t \leqslant 600$.

symmetry and asymmetric potentials. However, the soliton dynamics is changed by the shape of potential. The higher frequency results in a steep curve of potential in Fig. 3.20. On the contrary, the position and velocity change gently in Fig. 3.21.

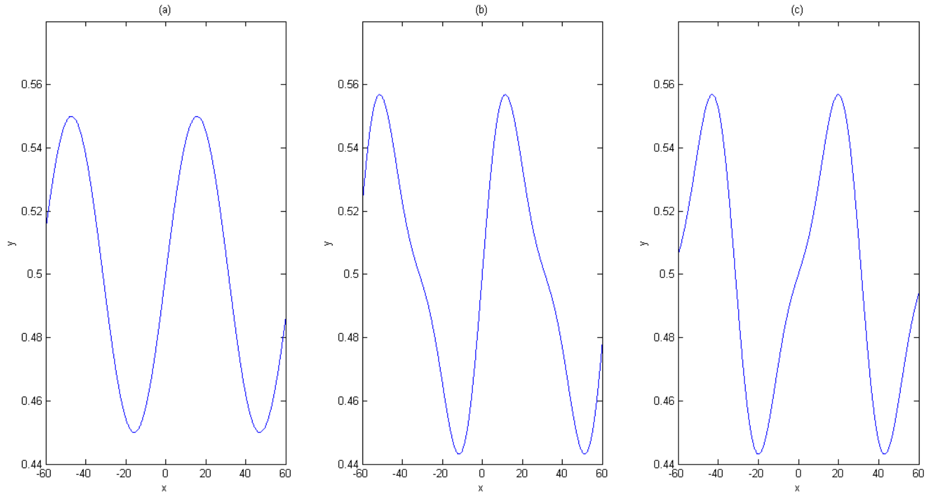

Figure 3.16: The regular symmetry potential (a) and the asymmetric potential (b) and (c).

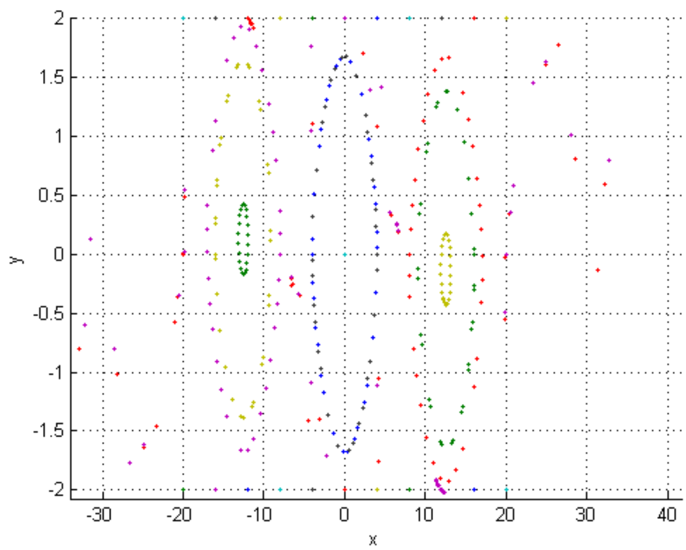

Figure 3.17: Poincare section of a soliton in an asymmetric potential. The potential is $W(x,t) = -\cos(k(t)x)$, $k(t) = k_0 + k_{mod}(\sin(\eta t) - 0.3\sin(2\eta t))$. The initial condition ranges are $-20 \leqslant x_0 \leqslant 20$, $-2 \leqslant v_0 \leqslant 2$, sampling by every $t = 2\pi/\eta$

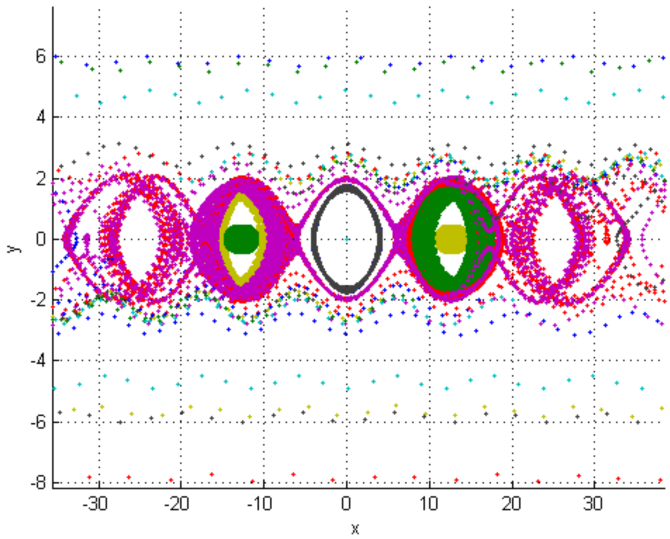

Figure 3.18: The trajectories of a soliton in an asymmetric potential. The potential is $W(x,t) = -\cos(k(t)x), k(t) = k_0 + k_{mod}(\sin(\eta t) - 0.3\sin(2\eta t))$. The initial condition ranges are $-20 \leqslant x_0 \leqslant 20$, $-2 \leqslant v_0 \leqslant 2$ sampling by every $t = 2\pi/100\eta$, $\eta = 0.1$.

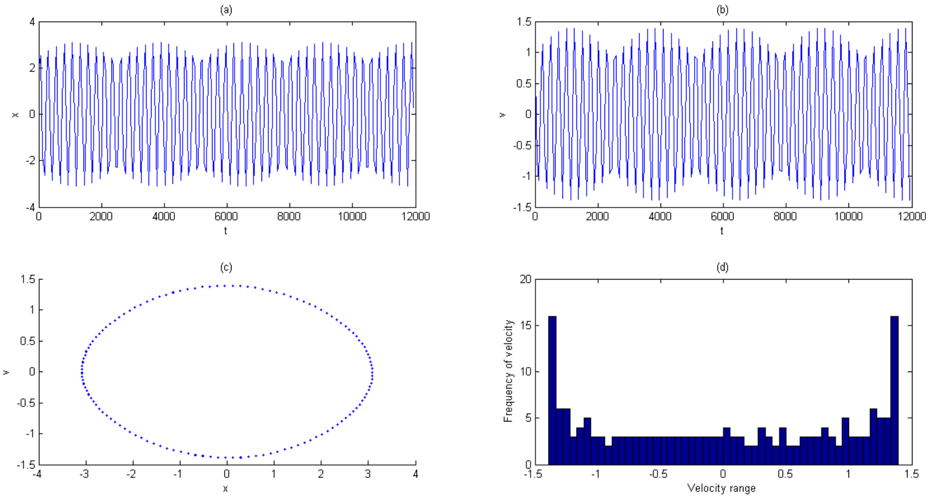

Figure 3.19: Soliton in the regular symmetry potential 3.16(a). The initial condition: $x_0 = 2$, $v_0 = 1$, (a) and (b) are trajectories of x and v respectively, (c) displays the Poincaré section sampling by every $t = 2\pi/\eta$, $\eta = 0.1$ during $t = 12000$. (d) shows the histogram of velocities.

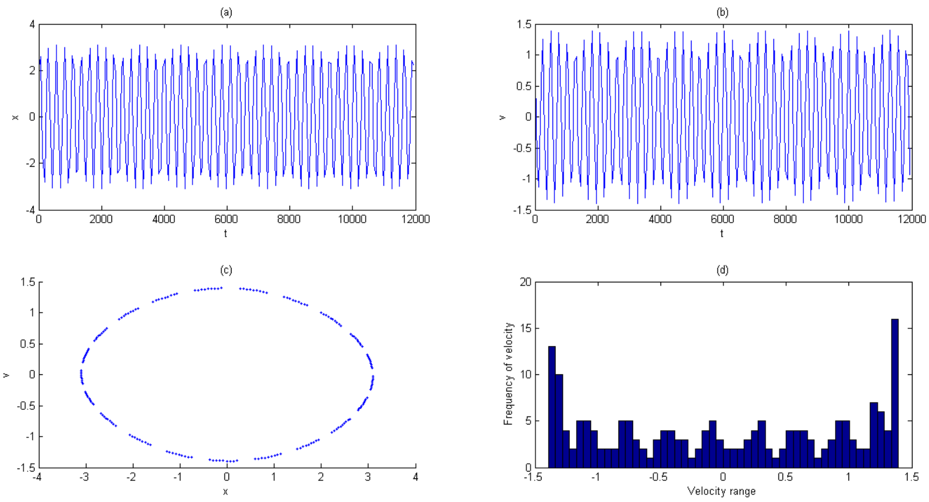

Figure 3.20: Soliton in the asymmetric potential 3.16(b). The initial condition: $x_0 = 2$, $v_0 = 1$, (a) and (b) are trajectories of x and v respectively, (c) displays the Poincaré section sampling by every $t = 2\pi/\eta$, $\eta = 0.1$ during $t = 12000$. (d) shows the histogram of velocities.

3.5 Damping

By adding a damping factor, equation (3.1) becomes:

$$\ddot{x}_0 + \alpha \dot{x}_0 + \frac{\pi}{2} w k(t)^2 \sin\left(k(t) x_0(t)\right) \operatorname{csch}\left(\frac{w\pi k(t)}{2}\right) = 0, \tag{3.4}$$

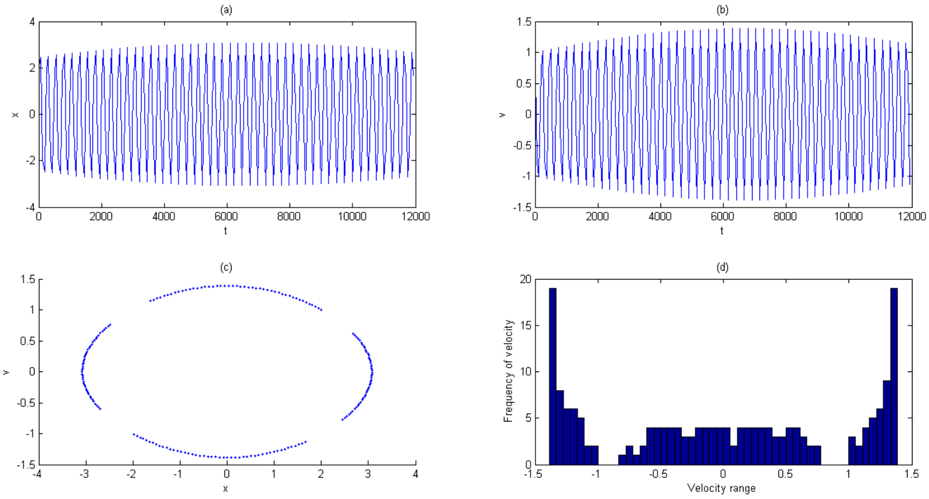

Figure 3.21: Soliton in the asymmetric potential 3.16(c). The initial condition: $x_0 = 2$, $v_0 = 1$, (a) and (b) are trajectories of x and v respectively, (c) displays the Poincaré section sampling by every $t = 2\pi/\eta$, $\eta = 0.1$ during $t = 12000$. (d) shows the histogram of velocities.

where α is the damping coefficient.

We studied this damping potential with three initial conditions: a small velocity near the centre (Fig.3.22-3.23); approaching the maximum potential with low speed (Fig.3.24); and a relatively higher velocity close to the potential minimum (Fig. 3.25). The results show that the soliton is oscillating in a potential well with a low speed.

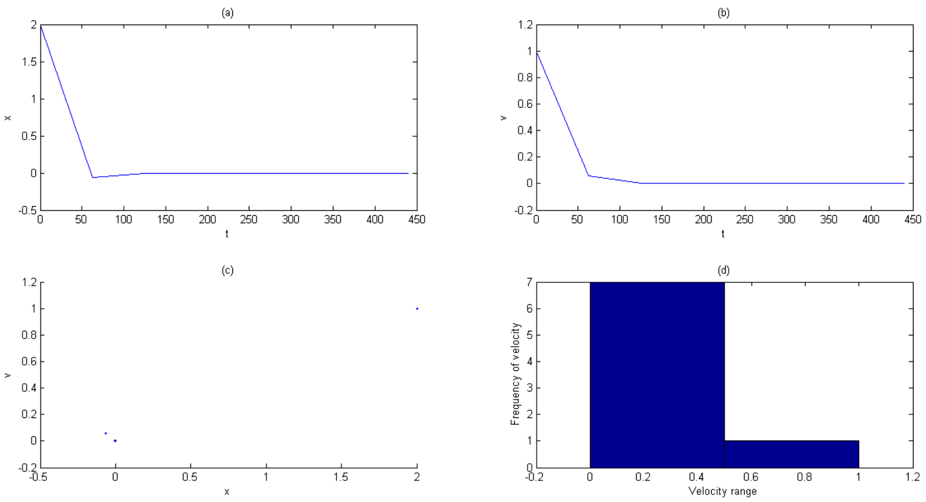

Figure 3.22: The damping case which initial condition: $x_0 = 2$, $v_0 = 1$ and $t = 500$, (a) and (b) are trajectories of x and v respectively, (c) displays the Poincaré section sampling by every $t = 2\pi/\eta$, $\eta = 0.1$. (d) shows the histogram of velocities.

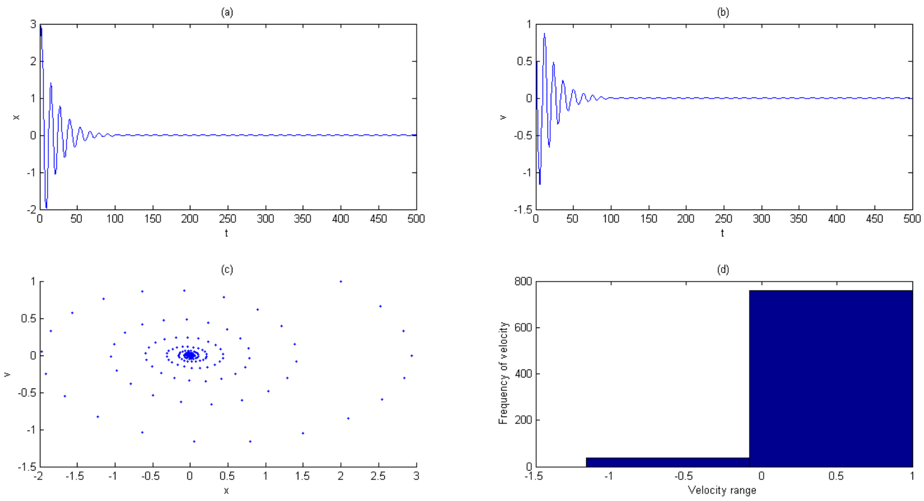

Figure 3.23: The damping case which initial condition: $x_0 = 2$, $v_0 = 1$ and $t = 500$ (a) and (b) are trajectories of x and v respectively, (c) displays the trajectories sampling by every $t = 2\pi/100\eta$, $\eta = 0.1$. (d) shows the histogram of velocities.

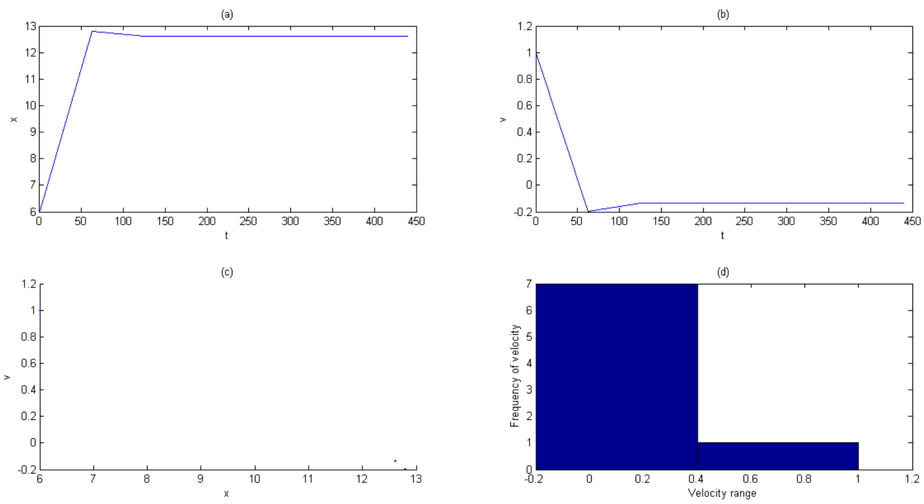

Figure 3.24: The damping case which initial condition: $x_0 = 6$, $v_0 = 1$ and $t = 500$ (a) and (b) are trajectories of x and v respectively, (c) displays the Poincaré section sampling by every $t = 2\pi/\eta$, $\eta = 0.1$. (d) shows the histogram of velocities.

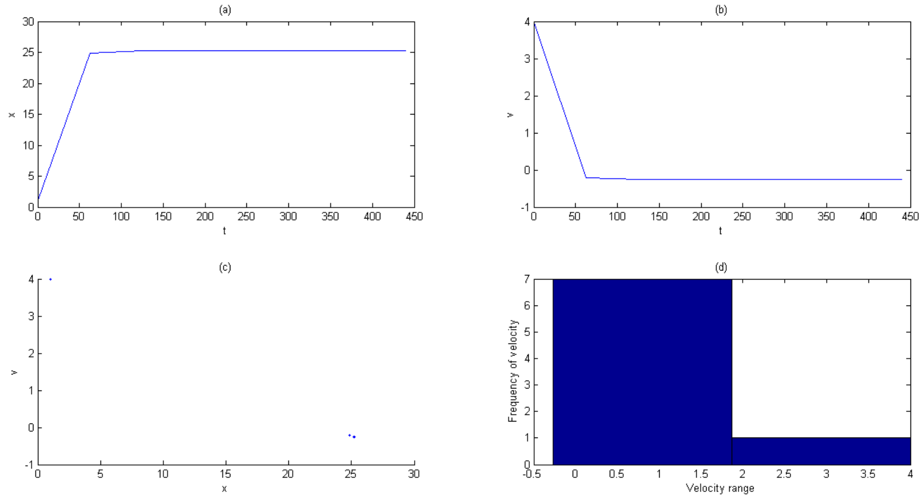

Figure 3.25: The damping case which initial condition: $x_0 = 1$, $v_0 = 4$ and $t = 500$ (a) and (b) are trajectories of x and v respectively, (c) displays the Poincaré section sampling by every $t = 2\pi/\eta$, $\eta = 0.1$. (d) shows the histogram of velocities.

3.6 Conclusion

We extend our research on soliton in time dependent potentials in this chapter. In the first place, the parameters of initial conditions are modulated. Thus, there are two situations: (i) soliton oscillations in the minimum of the potential, (ii) soliton jumping between potential wells. More details of position x and velocity v are provided by the Poincaré section and the histogram. Secondly, the parameter η in equation (2.2) is changed to $\eta = 1$, so that the driving frequency is double the potential frequency. Hence, we obtain a parametric resonance case. After that, by adding a new factor in the potential equation (2.2), we have another two scenarios: solitons in an asymmetric potential given by the inclusion of the term $\pm 0.3 \sin(2\eta t)$, and a damping term $\alpha \dot{x_0}$. In the damping case, we find that the soliton is oscillating with a tiny velocity in a potential well, no matter where the initial position is and how fast the initial speed is.

Chapter 4

Conclusion and future work

We have studied soliton dynamics in both time-independent and time-dependent potentials. We took advantage of the variational approach which helped to lessen the complexity of the problem by reducing it to the study of the dynamics of a particle in an effective potential. Generally, good agreement between the numerical and approximate variational solution was achieved, indicating the variational method is a simple yet powerful method for the study of soliton dynamics in a frequency-modulated potential. Several cases were discussed, including soliton trapping by a periodic potential, 'jumping' between adjacent wells and parametric resonance. Finally, we investigated the soliton dynamics by using Poincaré sections and histograms in several interesting potentials, including asymmetry and damping.

4.1 Concluding remarks

Chapter 1 provided the general background of a soliton in a potential. A review of previous studies was presented, for instance, the history of solitons, soliton in time-independent and time-dependent potentials, especially, the construction of periodic time-dependent potentials in experiment. We focused our discussion on the soliton dynamics in time-varying potentials.

Chapter 2 introduced our research model the nonlinear Schrödinger equation. Before the numerical methods and variational approach, a series of assumptions is discussed. These assumptions allow us to use an exact solution as initial condition for 'numerical propagation.' Also, we can treat the soliton as a particle in a variational method. Two simple cases are tested in the final section in this chapter. Thus, our variational approach provides a simple and useful tool.

Chapter 3 extended the research into the time-dependent dynamics. After finding and discussing two particular cases, 'jumping' between adjacent wells and parametric resonance, a further study is presented by four interesting dynamical cases: regular motion, parametric resonance, asymmetric potential and damping. Meanwhile, we introduced an important dynamic analysis tool: the Poincaré section.

Therefore, we create a better understanding of soliton dynamics in time-varying potential using different approaches.

4.2 Future work

In the following subsections, we will list a few aspects that could be interesting directions for future study.

4.2.1 Characterisation of velocity probability distribution

The aim of this research is to understand the soliton dynamics. In the future, we can also build a model for the velocity probability distribution and then predict the motion priorities of solitons. In particular, we should be capable to explain the behavoir of observed phenomena, such as the velocity distribution, and summarise them with a model or mathematical expression and expand the model to more scenarios of soliton dynamics. After the first step of collecting numbers of Poincaré sections, we should move forward a step to forecast with the built system and finally control it. Therefore, it is necessary to continue our research on modelling, forecasting and characterization the velocity probability distribution. Furthermore, we can restrain soliton's inherent instability-prone dynamics to guarantee oscillation stability, by using active structural control techniques [37].

4.2.2 Exploration of dynamics for different values of the parameters

We have studied several parameters in the modulated potential scenarios in the previous chapter and derived from (2.2)

$$W(x,t) = -\cos\left(k(t)x\right)\ , \quad k(t) = k_0 + k_{mod}\sin(\eta t)\ ,$$

In this equation, we can obtain different potentials by changing values of the parameters. For instance, when we set $\eta = 1$, we have a parametric resonance as presented in section 3.3. Also, we can break the shape symmetry of the potential by adding a factor studied in section 3.4. Similarly, we can explore diverse potentials in future work by changing the value of k_0, k_{mod} and η individually, or, for instance, setting η as a function to gain a time period symmetric potential.

4.2.3 Emergence of directed transport for particle

We examined the soliton dynamics in an asymmetric potential or damping in section 3.4 and 3.5 respectively. In a future study, it would be an interesting approach to study dynamics in the presence of both asymmetric potential and damping. For instance, whether or not these two resultant potentials are capable to 'collect' solitons or particles at the minimum of the potential. One possible application of this approach into practice is that particles, rather than solitons, can be trapped by optical tweezers, just in the same way as the solitons being trapped by light potentials.

We did not include these three aspects in our research. Nevertheless, it is worth to continue studying these.

4.2.4 Stochastic variations in the period of the lattice

In a physical system there is always some noise. If we extend our analysis to stochastic variations in the period of the lattice, it would be helpful to know how small the perturbations have to be for the effects to be negligible. The noise may have some effect on the stability on transitions between the different scenarios.

References

[1] A. Mourachkine, "Nonlinear excitations: Solitons," *High-Temperature Superconductivity in Cuprates: The Nonlinear Mechanism and Tunneling Measurements*, pp. 101–142, 2002.

[2] O. Morsch and M. Oberthaler, "Dynamics of Bose-Einstein condensates in optical lattices," *Rev. Mod. Phys.*, vol. 78, pp. 179–215, Feb 2006. `http://link.aps.org/doi/10.1103/RevModPhys.78.179`.

[3] N. J. Zabusky and M. D. Kruskal, "Interaction of 'solitons' in a collisionless plasma and the recurrence of initial states," *Phys. Rev. Lett.*, vol. 15, pp. 240–243, Aug 1965. `http://link.aps.org/doi/10.1103/PhysRevLett.15.240`.

[4] J. S. Russell, "Report on waves," in *14th meeting of the British Association for the Advancement of Science*, pp. 311–390, 1844.

[5] L. Munteanu and S. Donescu, *Introduction to soliton theory: applications to mechanics*, vol. 143. Springer, 2004.

[6] C. S. Gardner, J. M. Greene, M. D. Kruskal, and R. M. Miura, "Method for solving the Korteweg-DeVries equation," *Phys. Rev. Lett.*, vol. 19, pp. 1095–1097, Nov 1967. `http://link.aps.org/doi/10.1103/PhysRevLett.19.1095`.

[7] P. G. Drazin and R. S. Johnson, *Solitons: an introduction*, vol. 2. Cambridge University Press, 1989.

[8] J. R. Taylor, *Optical solitons: theory and experiment*, vol. 10. Cambridge University Press, 1992.

[9] D. J. Korteweg and G. De Vries, "Xli. on the change of form of long waves advancing in a rectangular canal, and on a new type of long stationary waves," *The London, Edinburgh, and Dublin Philosophical Magazine and Journal of Science*, vol. 39, no. 240, pp. 422–443, 1895.

[10] R. Y. Chiao, E. Garmire, and C. H. Townes, "Self-trapping of optical beams," *Phys. Rev. Lett.*, vol. 13, pp. 479–482, Oct 1964. `http://link.aps.org/doi/10.1103/PhysRevLett.13.479`.

[11] T. B. Benjamin and J. Feir, "The disintegration of wave trains on deep water part 1. theory," *Journal of Fluid Mechanics*, vol. 27, no. 03, pp. 417–430, 1967.

[12] H. A. Haus and W. S. Wong, "Solitons in optical communications," *Reviews of Modern Physics*, vol. 68, no. 2, pp. 423–444, 1996.

[13] H. Ishkhanyan, A. Manukyan, and A. Ishkhanyan, “Matter wave propagation above a step potential within the cubic-nonlinear Schrödinger equation,” in *International Journal of Modern Physics: Conference Series*, vol. 15, pp. 232–239, World Scientific, 2012.

[14] C. K. Jones and R. Marangell, “The spectrum of travelling wave solutions to the sine-gordon equation.,” *Discrete & Continuous Dynamical Systems-Series S*, vol. 5, no. 5, 2012.

[15] I. P. Herman, *Physics of the human body.* Springer Verlag Berlin Heidelberg, 2007.

[16] M. H. Anderson, J. R. Ensher, M. R. Matthews, C. E. Wieman, E. A. Cornell, *et al.*, “Observation of Bose-Einstein condensation in a dilute atomic vapor,” *science*, vol. 269, no. 5221, pp. 198–201, 1995.

[17] C. C. Bradley, C. A. Sackett, J. J. Tollett, and R. G. Hulet, “Evidence of Bose-Einstein condensation in an atomic gas with attractive interactions,” *Phys. Rev. Lett.*, vol. 75, pp. 1687–1690, Aug 1995. `http://link.aps.org/doi/10.1103/PhysRevLett.75.1687`.

[18] K. B. Davis, M. O. Mewes, M. R. Andrews, N. J. van Druten, D. S. Durfee, D. M. Kurn, and W. Ketterle, “Bose-Einstein condensation in a gas of sodium atoms,” *Phys. Rev. Lett.*, vol. 75, pp. 3969–3973, Nov 1995. `http://link.aps.org/doi/10.1103/PhysRevLett.75.3969`.

[19] D. Poletti, T. J. Alexander, E. A. Ostrovskaya, B. Li, and Y. S. Kivshar, “Dynamics of matter-wave solitons in a ratchet potential,” *Phys. Rev. Lett.*, vol. 101, p. 150403, Oct 2008. `http://link.aps.org/doi/10.1103/PhysRevLett.101.150403`.

[20] G. Agrawal, *Nonlinear Fiber Optics.* Academic Press, San Diego, 1995.

[21] K. E. Strecker, G. B. Partridge, A. G. Truscott, and R. G. Hulet, “Formation and propagation of matter-wave soliton trains,” *Nature*, vol. 417, no. 6885, pp. 150–153, 2002. `http://dx.doi.org/10.1038/nature747`.

[22] M. A. Porter, M. Chugunova, and D. E. Pelinovsky, “Feshbach resonance management of Bose-Einstein condensates in optical lattices,” *Physical Review E*, vol. 74, no. 3, p. 036610, 2006.

[23] I. Bloch, “Ultracold quantum gases in optical lattices,” *Nature Physics*, vol. 1, no. 1, pp. 23–30, 2005.

[24] P. Papagiannis, Y. Kominis, and K. Hizanidis, “Power and momentum dependent soliton dynamics in lattices with longitudinal modulation,” *Phys. Rev. A*, vol. 84, p. 013820, Jul 2011. `http://link.aps.org/doi/10.1103/PhysRevA.84.013820`.

[25] N. K. Efremidis and D. N. Christodoulides, "Lattice solitons in Bose-Einstein condensates," *Phys. Rev. A*, vol. 67, p. 063608, Jun 2003. `http://link.aps.org/doi/10.1103/PhysRevA.67.063608`.

[26] Z. Ai-Xia and X. Ju-Kui, "Dynamics of bright/dark solitons in bose–einstein condensates with time-dependent scattering length and external potential," *Chinese Physics Letters*, vol. 25, no. 1, p. 39, 2008.

[27] B. Baizakov, G. Filatrella, B. Malomed, and M. Salerno, "Double parametric resonance for matter-wave solitons in a time-modulated trap," *Phys. Rev. E*, vol. 71, p. 036619, Mar 2005. `http://link.aps.org/doi/10.1103/PhysRevE.71.036619`.

[28] T. Belyaeva, V. Serkin, C. Hernandez-Tenorio, and L. Kovachev, "Soliton dynamics in confining time-dependent potentials," in *15th International School on Quantum Electronics: Laser Physics and Applications*, pp. 70271I–70271I, International Society for Optics and Photonics, 2008.

[29] J. Abdullaev, D. Poletti, E. A. Ostrovskaya, and Y. S. Kivshar, "Controlled transport of matter waves in two-dimensional optical lattices," *Phys. Rev. Lett.*, vol. 105, p. 090401, Aug 2010. `http://link.aps.org/doi/10.1103/PhysRevLett.105.090401`.

[30] D. Anderson, "Variational approach to nonlinear pulse propagation in optical fibers," *Phys. Rev. A*, vol. 27, pp. 3135–3145, Jun 1983. `http://link.aps.org/doi/10.1103/PhysRevA.27.3135`.

[31] A. Hasegawa and F. Tappert, "Transmission of stationary nonlinear optical pulses in dispersive dielectric fibers. i. anomalous dispersion," *Applied Physics Letters*, vol. 23, no. 3, pp. 142–144, 1973.

[32] J. Weideman and B. Herbst, "Split-step methods for the solution of the nonlinear Schrödinger equation," *SIAM Journal on Numerical Analysis*, vol. 23, no. 3, pp. 485–507, 1986.

[33] T. J. Alexander, K. Heenan, M. Salerno, and E. A. Ostrovskaya, "Dynamics of matter-wave solitons in harmonic traps with flashing optical lattices," *Phys. Rev. A*, vol. 85, p. 063626, Jun 2012. `http://link.aps.org/doi/10.1103/PhysRevA.85.063626`.

[34] K. Pearson, "Contributions to the mathematical theory of evolution. II. skew variation in homogeneous material," *Philosophical Transactions. Royal Society of London. Series A. Mathematical and Physical Sciences.*, vol. 186, pp. 343–414, 1895.

[35] N. McLachlan, *Theory and Application of Mathieu Functions.* Dover Publication, NY, 1964.

[36] A. Nayfeh and D. Mook, *Nonlinear Oscillations.* Wiley-Interscience, 1979.

[37] W. F. Andress, D. S. Ricketts, X. Li, and D. Ham, “Passive & active control of regenerative standing & soliton waves,” in *Custom Integrated Circuits Conference, 2006. CICC’06. IEEE*, pp. 29–36, IEEE, 2006.

Appendix A

Matlab code

A.1 Numerical method (PDE)

```
clear;
L=5;
N=2^12;

%n=8; % mass of soliton
%n=5;
x0=2;
%x0=0;  % initial position
V=0;     % speed of soliton

w0=sqrt(0.2);
%    k0=0.5;
%    kmod=0;
%
%    lattfreq = 0.1;
%t=0;
 %lattamp=1;
% data1=[];
% data2=[];
%for A=0.4:0.2:1;
A=8;
W=1/A;
tfin = 20.0; %500.0;

dx=2*L/N;
dt=dx^2; %0.00001;
tout = 10*dt;
itmax = tfin/dt;
tcheck = tout/dt;
```

```
Nt = floor(tfin/tout)+1;
tp=0:tout:tfin;

% a=4;
x=-L:dx:L-dx;
%[X,T]=meshgrid(x,tp);

%y=(n./2).*sech((n./2)*(x-x0)).*exp(i*V.*x0);  %solution of
    Schrodinger equation
%y=sqrt(2*a).*sech((x-x1).*sqrt(a));
y=A*sech((x-x0)/W).*exp(1i*V.*x0);  %Stationary solution

 figure(1);
 plot(x,abs(y))
 xlabel('x');
 ylabel('|\psi|');
 title('Soliton')
axis([-L L 0 1])
plot(x,abs(y))
xlabel('x');
ylabel('|\psi|');
grid on


k=[0:N/2-1 0 -N/2+1:-1];
K=2*k*pi/(2*L);
u=zeros(N,Nt);
tpos = 1;
u(:,tpos) = y;
tpos = tpos+1;

res=[]; % result vector for storing maximums

for j=1:itmax,
    t=j*dt;
    %v=-cos((k0+kmod.*sin(lattfreq.*t)).*x);
    z=fft(y);
    g=exp(-(1/2)*1i*K.*K.*dt);
    G=z.*g;
```

```
        F=ifft(G);
        H=(abs(F)).^2;
        y=F.*exp(1i*(H-v)*dt);
        %y=F.*exp(1i*H*dt);
        %y=F.*exp(i*H*dt-i*vv);
        [val pos]=max(abs(y)); % val = peak , pos= element number of peak
        res=[res; t x(pos)]; % save time and x position of peak
        if mod(j,tcheck) == 0
            u(:,tpos) = y;
            tpos = tpos+1;
        end
end



%        figure(3);
%        imagesc(x,tp,abs(u'));
%        shading interp
%        colormap(jet)
%        xlabel('|\psi|');
%        ylabel('t');
%        set(gca,'XAxisLocation','top');
%        set(gca,'YDir','reverse');
%print -dpng qwe1
%figure
%plot(res(:,1),res(:,2)) % plot peak position


M=max(abs(u));

xx=linspace(min(x),max(x),N*5);
U=interp2(x,tp,abs(u'),xx,tp');

%res1=[res; M];
    % figure(2);
%        subplot(1,2,1)
% plot(x,abs(y))
% xlabel('x');
```

```
% ylabel('|\psi|');
% title('Soliton')

     %subplot(1,2,1)
     figure();
     imagesc(xx,tp',U);
     shading interp
     colormap(jet)
     xlabel('|\psi|');
     ylabel('t');
     title('Soliton propagation')
   set(gca,'XAxisLocation','top');
     set(gca,'YDir','reverse');

 colorbar% figure()
  subplot(1,2,2)
  contour(x,tp,abs(u'),[0.5 1 A])
  xlabel('|\psi|');
  ylabel('t');
  title('Contour of Soliton propagation')
  set(gca,'XAxisLocation','top');
  set(gca,'YDir','reverse');

  print -dpng qwe2

  data1=[data1;M];
 data2=[data2;W max(M) min(M) max(M)-min(M)];
% figure(3)
% subplot(1,2,2)
% plot(tp',M);
% xlabel('t');
% ylabel('Max|\psi|');
% axis([0 10 0 8.5])
% title('Max|\psi| vs t')
% hold on
%
% figure(4)
% plot(W,max(M)-min(M),'-ob');
% xlabel('Width');
```

```
% ylabel('D-value')
% title('D-value vs t')
% hold on
%end
```

A.2 Variational approach (ODE)

Function

```
function dy = nlfunc2(t,y)

% Control parameters (defined in the scripts "bifplot.m", "trajplot.m" and
% "poincare.m"
global omega;
global lattamp;
global k0;
global lattfreq;
global kmod;
%global num;
global W;
global alpha;

dy = zeros(2,1);     % a column vector
%lattarg = (k0+kmod*(sin(lattfreq*t)+0.3*sin(2*lattfreq*t))); % asymmetry;
lattarg = (k0+kmod*sin(lattfreq*t));
% The nonlinear equations in first-order ODE form.
dy(1) = y(2);
dy(2) = -omega^2*y(1)-lattamp*(pi/2)*lattarg^2*W*(sin(lattarg*y(1)))*csch(pi*lattarg*W/2);
%dy(2) = -omega^2*y(1)-alpha*dy(1)-lattamp*(pi/2)*lattarg^2*W*(sin(lattarg*y(1)))*csch(pi*lattarg*W/2); %damping
```

Trajectory

```
% Script to plot the trajectory from t=tstart until t=tfin, using the initial
% conditions x=xinit and y=yinit and integrating the system of nonlinear
% first-order ODEs defined in nlfunc. The Matlab routine "comet" is used to
```

```
% make visualization of the trajectory easier.


% Options for ODE integrator, including the numerical error
    tolerances (see
% the Matlab help manual for details)
options = odeset('RelTol',1e-6,'AbsTol',[1e-11 1e-11]);

% The control parameters used by the specific function
    defined in nlfunc
global omega;
global lattamp;
global k0;
global lattfreq;
global kmod;
%global num;
global W

% The values of the control parameters
omega = 0;%sqrt(0.2);
lattamp = 1;
%num = 5.0;
k0 = 0.5;
kmod = 0.05;
lattfreq = 1;
W=0.25;
% The initial conditions
xinit = 0.5;
vinit = 0.0;

% The start and finish times for the integration
tstart = 0.0;
tfin = 300.0;
timestep = 0.01;
tsamp=[tstart:timestep:tfin];


% The Matlab integrator (Runge-Kutta)
```

```
%[T,Y] = ode45(@nlfunc2,[tstart tfin],[xinit vinit],options);
[T,Y] = ode45(@nlfunc2,tsamp,[xinit vinit],options);

% Plot of the evolution
figure()
%plot(Y(:,1),T,'-',Y(:,2),T,'-.')
plot(Y(:,1),T,'-')
%xlabel('x,dx/dt');
xlabel('x')
ylabel('t');
 set(gca,'XAxisLocation','top');
 set(gca,'YDir','reverse');
%axis([-25 25 0 tfin])

% figure()
% plot(Y(:,1),T,'-',Y(:,2),T,'-.')
% plot(T,Y(:,2),'-')
% xlabel('x,dx/dt');
% xlabel('t')
% ylabel('v');
% set(gca,'XAxisLocation','top');
% set(gca,'YDir','reverse');
% Plot of the trajectory in the 2D phase space
% figure(2)
% plot(abs(Y(:,1)).^2,abs(Y(:,2)).^2)
% xlabel('x');
% ylabel('y');
%
% Prettier display of the trajectory in the phase space
% figure(3)
% comet(abs(Y(:,1)).^2,abs(Y(:,2)).^2)
```

Poincaré section

```
% Script to plot the Poincare map of the system defined in nlfunc.
% Integration of the system begins at t = tstart, however data for the map
```

```
% is not taken until t = ttrans to try and avoid initial
    transient
% behaviour.  The evolution of the system vs. time is also
    plotted.

% Options for ODE integrator, including the numerical error
    tolerances (see
% the Matlab help manual for details)
options = odeset('RelTol',1e-10,'AbsTol',[1e-11 1e-11]);

% The control parameters used by the specific function
    defined in nlfunc
global omega;
global lattamp;
global k0;
global lattfreq;
global kmod;
%global num;
global M; %mass
global W

% The values of the control parameters
omega = 0;
lattamp = 1;
%num = 5.0;
k0 = 0.5;
kmod = 0.05;
lattfreq = 0.1;
W=0.25;
M=8;
% The initial conditions
% xinit = 0.2;
% vinit = 0.0;

% The start and finish times for the integration and time
    integrated before
% recording the map (to avoid transients)
tstart = 0.0;
tfin = 2000.0;
```

```
ttrans = 0.0;
xmin = -20;
xmax = 20;
dx = 4;
vmin = -2.0;
vmax = 2.0;
dv = 2;
xinittot = [xmin:dx:xmax];
imax = length(xinittot);
vinittot = [vmin:dv:vmax];
jmax = length(vinittot);
n = imax*jmax;
tforce = 2.0*pi/lattfreq;
% The sample period for the Poincare map (determined by the
    driving frequency)
%for T0=1:2
timestep = tforce;
%timestep = T0+2.0*pi/k0;
%timestep = 2.0*pi/lattfreq;

% The time points of the Poincare map
tsamp=[tstart:timestep:tfin];

% Total number of sample points
ntot = length(tsamp);
ii = 99;
% Number of points discarded to avoid transients (cast into
    integer form)
ntrans = cast((ttrans-tstart)/timestep,'int32')+1;
R=[];
%R=zeros(ntot,3,n);
% The Matlab integrator (Runge-Kutta)
xinit = xinittot(1);
vinit = vinittot(1);
[T,Y] = ode45(@nlfunc2,tsamp,[xinit vinit],options);

% Plot of the evolution
% figure(1)
% plot(T,Y(:,1),'-',T,Y(:,2),'-.')
```

```
% xlabel('t');
% ylabel('x, y');

% Plot of the Poincare map, starting the map after some time
    t_trans to
% avoid the transients
figure(2)
hold on
scatter(Y(ntrans:ntot,1),Y(ntrans:ntot,2),5,'filled')
%plot3(Y(ntrans:ntot,1),Y(ntrans:ntot,2),T);
grid on
xlabel('x');
ylabel('y');
%zlabel('t');

 Rdata1=[];

for i=1:imax
    for j = 1:jmax
     xinit = xinittot(i);
     vinit = vinittot(j);
      [T,Y] = ode45(@nlfunc2,tsamp,[xinit vinit],options);
     scatter(Y(ntrans:ntot,1),Y(ntrans:ntot,2),5,'filled');
      R = [R;Y(ntrans:ntot,1),Y(ntrans:ntot,2),T];%x,v,t

    end
end
R1=reshape(R(:,1),ntot,n); %x
R2=reshape(R(:,2),ntot,n);%v
MR1 = mean(R1); % tot mean x
MR2 = mean(R2); % tot mean v
sdv = std(R2);% standard deviations of v
Rdata1=[Rdata1; MR1 MR2 sdv];
%end
```

Damping

```
% Script to plot the Poincare map of the system defined in
   nlfunc.
```

```
% Integration of the system begins at t = tstart , however data for the map
% is not taken until t = ttrans to try and avoid initial transient
% behaviour.  The evolution of the system vs. time is also plotted.

% Options for ODE integrator, including the numerical error tolerances (see
% the Matlab help manual for details)
options = odeset('RelTol',1e-10,'AbsTol',[1e-11 1e-11]);

% The control parameters used by the specific function defined in nlfunc
global omega;
global lattamp;
global k0;
global lattfreq;
global kmod;
global M; %mass
global W
global alpha;

% The values of the control parameters
omega = 0;
lattamp = 1;
alpha =0.1;
%num = 5.0;
k0 = 0.5;
kmod = 0.05;
lattfreq = 0.1;
W=0.25;
M=8;
% The initial conditions
% xinit = 0.2;
% vinit = 0.0;

% The start and finish times for the integration and time integrated before
```

```
% recording the map (to avoid transients)
tstart = 0.0;
tfin = 3000.0;
ttrans = 0.0;
xmin = -10;
xmax = 10;
dx = 4;
vmin = -2.0;
vmax = 2.0;
dv = 1;
xinittot = [xmin:dx:xmax];
imax = length(xinittot);
vinittot = [vmin:dv:vmax];
jmax = length(vinittot);
n = imax*jmax;
tforce = 2.0*pi/lattfreq;
% The sample period for the Poincare map (determined by the
    driving frequency)
%for T0=1:2
timestep = tforce;
%timestep = T0+2.0*pi/k0;
%timestep = 2.0*pi/lattfreq;

% The time points of the Poincare map
tsamp=[tstart:timestep:tfin];

% Total number of sample points
ntot = length(tsamp);
%ii = 99;
% Number of points discarded to avoid transients (cast into
    integer form)
ntrans = cast((ttrans-tstart)/timestep,'int32')+1;
R=[];
%R=zeros(ntot,3,n);
% The Matlab integrator (Runge-Kutta)
xinit = xinittot(1);
vinit = vinittot(1);
[T,Y] = ode45(@nlfunc2,tsamp,[xinit vinit],options);

```

```
% Plot of the evolution
% figure(1)
% plot(T,Y(:,1),'-',T,Y(:,2),'-.')
% xlabel('t');
% ylabel('x, y');

% Plot of the Poincare map, starting the map after some time
    t_trans to
% avoid the transients
figure()
hold on
scatter(Y(ntrans:ntot,1),Y(ntrans:ntot,2),5,'filled')
%plot3(Y(ntrans:ntot,1),Y(ntrans:ntot,2),T);
grid on
xlabel('x');
ylabel('y');
axis([-100 100 -5 5])
%zlabel('t');

 Rdata1=[];

for i=1:imax
    for j = 1:jmax
     xinit = xinittot(i);
     vinit = vinittot(j);
      [T,Y] = ode45(@nlfunc22,tsamp,[xinit vinit],options);
     scatter(Y(ntrans:ntot,1),Y(ntrans:ntot,2),5,'filled');
      R = [R;Y(ntrans:ntot,1),Y(ntrans:ntot,2),T];%x,v,t

    end
end
R1=reshape(R(:,1),ntot,n); %x
R2=reshape(R(:,2),ntot,n);%v
MR1 = mean(R1); % tot mean x
MR2 = mean(R2); % tot mean v
sdv = std(R2);% standard deviations of v
Rdata1=[Rdata1; MR1 MR2 sdv];
```

Appendix B

Numerics

Width	Max|ψ|	Min|ψ|	D-value
2.5	0.400009	0.399983	2.63E-05
1.666667	0.6	0.599989	1.08E-05
1.25	0.800009	0.799974	3.48E-05
1	1.000022	0.99995	7.19E-05
0.833333	1.200037	1.199914	0.000123
0.714286	1.400059	1.399863	0.000196
0.625	1.600087	1.599795	0.000292
0.555556	1.800124	1.799709	0.000415
0.5	2.00017	1.9996	0.00057
0.454545	2.200226	2.199468	0.000758
0.416667	2.400293	2.399309	0.000985
0.384615	2.600372	2.599124	0.001248
0.357143	2.800463	2.798901	0.001562
0.333333	3.000569	2.998654	0.001915
0.3125	3.200689	3.198365	0.002323
0.294118	3.400823	3.39803	0.002794
0.277778	3.600972	3.597664	0.003307
0.263158	3.801149	3.797272	0.003877
0.25	4.001325	3.996855	0.00447
0.238095	4.201529	4.196346	0.005183
0.227273	4.401751	4.395754	0.005997
0.217391	4.601977	4.595115	0.006862
0.208333	4.80227	4.794431	0.007839
0.2	5.002575	4.993703	0.008872
0.192308	5.202808	5.192934	0.009874
0.185185	5.403219	5.392126	0.011093
0.178571	5.603461	5.591283	0.012179
0.172414	5.803967	5.790407	0.01356
0.166667	6.004205	5.989506	0.014699
0.16129	6.204728	6.188582	0.016145
0.15625	6.40526	6.387644	0.017615
0.151515	6.605475	6.586698	0.018776
0.147059	6.805918	6.785753	0.020164
0.142857	7.006763	6.984818	0.021945
0.138889	7.207331	7.183903	0.023428
0.135135	7.407524	7.38302	0.024503
0.131579	7.607248	7.582181	0.025067
0.128205	7.808523	7.7814	0.027124
0.125	8.009714	7.98069	0.029023

Figure B.1: No potential. The soliton width range $(0.125 - 2.5)$

0.5	2.000026	1.999944	8.18E-05
0.333333	3.000081	2.999811	0.00027
0.25	4.000192	3.999551	0.000641
0.2	5.000367	4.999156	0.001211
0.166667	6.000645	5.998716	0.001929
0.142857	7.001015	6.998398	0.002617
0.125	8.001394	7.998477	0.002917

Figure B.2: No potential. The soliton width range $(0.125 - 0.5)$

Width	Max|ψ|	Min|ψ|	D-value
2.5	0.903566	0.4	5.04E-01
1.666667	0.980556	0.6	3.81E-01
1.25	1.082849	0.798281	2.85E-01
1	1.207485	0.972256	2.35E-01
0.833333	1.351114	1.188076	0.163038
0.714286	1.512108	1.398238	0.11387
0.625	1.681198	1.6	0.081198
0.555556	1.860304	1.8	0.060304
0.5	2.048304	1.999943	0.048361
0.454545	2.23603	2.199852	0.036178
0.416667	2.42944	2.399726	0.029714
0.384615	2.622564	2.599563	0.023001
0.357143	2.818985	2.799359	0.019626
0.333333	3.015501	2.99911	0.01639
0.3125	3.212576	3.198817	0.013759
0.294118	3.410941	3.398476	0.012465
0.277778	3.610521	3.598088	0.012433
0.263158	3.809301	3.797651	0.01165
0.25	4.007005	3.997166	0.00984
0.238095	4.206562	4.196632	0.00993
0.227273	4.406315	4.395923	0.010392
0.217391	4.606512	4.595082	0.01143
0.208333	4.806591	4.794319	0.012273
0.2	5.006406	4.99403	0.012377
0.192308	5.207466	5.193269	0.014197
0.185185	5.409621	5.392469	0.017151
0.178571	5.610964	5.591633	0.01933
0.172414	5.809636	5.790765	0.018871
0.166667	6.008809	5.98987	0.018939
0.16129	6.213336	6.188952	0.024384
0.15625	6.41139	6.388019	0.023371
0.151515	6.613298	6.587071	0.026227
0.147059	6.814893	6.786136	0.028758
0.142857	7.015221	6.984615	0.030606
0.138889	7.215327	7.183449	0.031877
0.135135	7.417081	7.383409	0.033672
0.131579	7.614037	7.578667	0.03537
0.128205	7.818707	7.779153	0.039554
0.125	8.024533	7.980921	0.043612

Figure B.3: Time-independent parabolic potential. The soliton width range (0.125−2.5).

0.5	2.048301	2	4.83E-02
0.333333	3.014583	3	0.014583
0.25	4.006326	4	0.006326
0.2	5.003354	4.999765	0.003589
0.166667	6.002447	5.999364	0.003083
0.142857	7.002324	6.999029	0.003294
0.125	8.002767	7.998012	0.004755

Figure B.4: Time-independent parabolic potential. The soliton width range ($0.125-0.5$).

2.5	0.902267	0.4	5.02E-01
1.666667	0.980525	0.6	0.380525
1.25	1.082848	0.798297	0.284551
1	1.207492	0.972599	0.234893

Figure B.5: Time-independent parabolic potential. The soliton width range ($1-2.5$).

Width	Max|ψ|	Min|ψ|	D-value
2.5	0.75582	0.380727	3.75E-01
1.666667	0.929401	0.555634	3.74E-01
1.25	1.072388	0.773932	2.98E-01
1	1.213571	0.983066	2.31E-01
0.833333	1.362918	1.194439	0.168479
0.714286	1.523389	1.4	0.123389
0.625	1.693577	1.6	0.093577
0.555556	1.872392	1.8	0.072392
0.5	2.055522	1.999979	0.055543
0.454545	2.242862	2.199891	0.042971
0.416667	2.434013	2.399769	0.034244
0.384615	2.626886	2.599609	0.027277
0.357143	2.821616	2.799408	0.022208
0.333333	3.017744	2.999163	0.01858
0.3125	3.214825	3.198873	0.015952
0.294118	3.412495	3.398536	0.01396
0.277778	3.610709	3.59815	0.012558
0.263158	3.809279	3.797717	0.011563
0.25	4.008195	3.997234	0.010961
0.238095	4.207365	4.196704	0.010661
0.227273	4.406658	4.396125	0.010534
0.217391	4.606256	4.595499	0.010757
0.208333	4.805854	4.794827	0.011027
0.2	5.005738	4.994111	0.011627
0.192308	5.205609	5.193353	0.012256
0.185185	5.405583	5.392555	0.013028
0.178571	5.605889	5.591721	0.014168
0.172414	5.805761	5.790854	0.014906
0.166667	6.005969	5.98996	0.016009
0.16129	6.206354	6.189044	0.01731
0.15625	6.406558	6.388112	0.018446
0.151515	6.60654	6.587172	0.019368
0.147059	6.807237	6.786231	0.021006
0.142857	7.007859	6.985299	0.02256
0.138889	7.208222	7.184387	0.023835
0.135135	7.408228	7.383506	0.024723
0.131579	7.608181	7.582667	0.025514
0.128205	7.809421	7.781886	0.027535
0.125	8.010483	7.981175	0.029307

Figure B.6: Time-independent periodic potential. The soliton width range ($0.125-2.5$).

0.5	2.055524	2	5.55E-02
0.333333	3.017638	3	0.017638
0.25	4.007623	4	0.007623
0.2	5.00404	4.999916	0.004124
0.166667	6.002597	5.999525	0.003072
0.142857	7.001992	6.999202	0.00279
0.125	8.002226	7.999101	0.003125

Figure B.7: Time-independent periodic potential. The soliton width range $(0.125-0.5)$.

2.5	0.755798	0.381625	3.74E-01
1.666667	0.929395	0.5556	0.373795
1.25	1.072332	0.773917	0.298415
1	1.213571	0.983032	0.230539

Figure B.8: Time-independent periodic potential. The soliton width range $(1-2.5)$.

Width	Max|ψ|	Min|ψ|	D-value
0.25	4.006727	3.997763	8.96E-03

Figure B.9: Time-independent periodic potential. The soliton width $(w = 0.25)$. $W(x,t) = -\cos\left[k_0 + k_{mod}\sin(\eta t)\right]x$, $k_0 = 0.5$, $k_{mod} = 0$, and $x_0 = 2$.

Width	Max|ψ|	Min|ψ|	D-value
0.25	4.004859	3.998048	6.81E-03

Figure B.10: Time-independent periodic potential. The soliton width range $(w = 0.25)$. $W(x,t) = \dfrac{1}{2}\omega_0^2 x^2$, $\omega_0 = \sqrt{0.2}$ and $x_0 = 2$